Temperature dependent model for the quasi-static stick–slip process on a soft substrate

Stefano Giordano

Soft Matter

ARTICLE TYPE

Cite this: DOI: 00.0000/xxxxxxxxxx

Temperature dependent model for the quasi-static stick-slip process on a soft substrate

Stefano Giordano,[a]

Received Date
Accepted Date

DOI: 00.0000/xxxxxxxxxx

The classical Prandtl-Tomlinson model is the most famous and efficient method to describe the stick-slip phenomenon and the resulting friction between a slider and a corrugated substrate. It is widely used in all studies of frictional physics and notably in nanotribology. However, it considers a rigid or undeformable substrate and therefore is hardly applicable for investigating the physics of soft matter and in particular biophysics. For this reason, we introduce here a modified model that is capable of taking into consideration a soft or deformable substrate. It is realized by a sequence of elastically bound quadratic energy wells, which represent the corrugated substrate. We study the quasi-static behavior of the system through the equilibrium statistical mechanics. We thus determine the static friction and the deformation of the substrate as a function of temperature and substrate stiffness. The results are of interest for the study of cell motion in biophysics and for haptic and tactile systems in microtechnology.

1 Introduction

The friction between two contacting surfaces is often controlled by the stick-slip phenomenon, which has been observed and studied over a very wide range of scales.[1–5] Although the deep understanding of the underlying mechanisms is still incomplete, important progress has been made in the study of the nanoscale friction,[6–8] and the stick-slip effect in biological and soft structures,[9] including molecular motors,[10] cells spreading,[11] and articular joints motion,[12,13] just to name a few.

From the experimental point of view, a strong momentum for understanding the nanoscale friction and the stick-slip phenomenon has been provided by the introduction of the atomic force microscope,[14] and the surface force apparatus.[15] In parallel, computational investigations have been made possible by the development of efficient molecular dynamics algorithms and multiscale approaches.[16–18]

These experimental and numerical devices allowed the observation and the study of the characteristic stick-slip motion of a slider, interacting with a corrugated substrate. The latter can be thought of as a periodic potential composed of a sequence of energy wells (a sinusoidal potential is typically adopted). This conceptual scheme exactly corresponds to the so-called Prandtl-Tomlinson model,[19,20] pioneered in the early 20th century. Despite its age, it is still currently the most efficient model to describe stick-slip motion and nanoscale friction. It has therefore been studied intensively and its outcomes have often been compared with experiments and simulations.[21,22] A careful analysis of this model led to the discovery of different operating regimes of temperature and velocity and these theoretical conclusions have contributed to the interpretation of many atomic force microscope experiments.[23–33] Since the Prandtl-Tomlinson model considers only one particle sliding on the substrate, its natural generalization is to take into account a one-dimensional elastic chain of interacting particles moving over the periodic potential mimicking the substrate. This scheme, originally introduced to study the dislocations motion and explain the plastic deformation in crystals, is known as Frenkel-Kontorova model and perfectly describes the mutual sliding of two different crystalline surfaces.[34,35]

All earlier approaches based on the Prandtl-Tomlinson or Frenkel-Kontorova models have mostly considered a rigid or undeformable substrate and therefore are hardly applicable to soft matter systems or biological structures. To fill this gap, we develop here a theory for the rate-independent stick-slip phenomenon on a soft substrate, based on equilibrium statistical mechanics. It represents a sort of generalization of the Prandtl-Tomlinson model, able to take into consideration both the temperature effect and the influence of the deformable substrate stiffness. The model is developed here for a single sliding particle but can be easily generalized to the case of a Frenkel-Kontorova chain.

The possibility of determining the effects of substrate deformability on the properties of stick-slip motion and friction with a simple theoretical model is particularly important for studying the

[a] Univ. Lille, CNRS, Centrale Lille, Univ. Polytechnique Hauts-de-France, UMR 8520 - IEMN - Institut d'Electronique de Microélectronique et de Nanotechnologie, F-59000 Lille, France. E-mail: stefano.giordano@univ-lille.fr

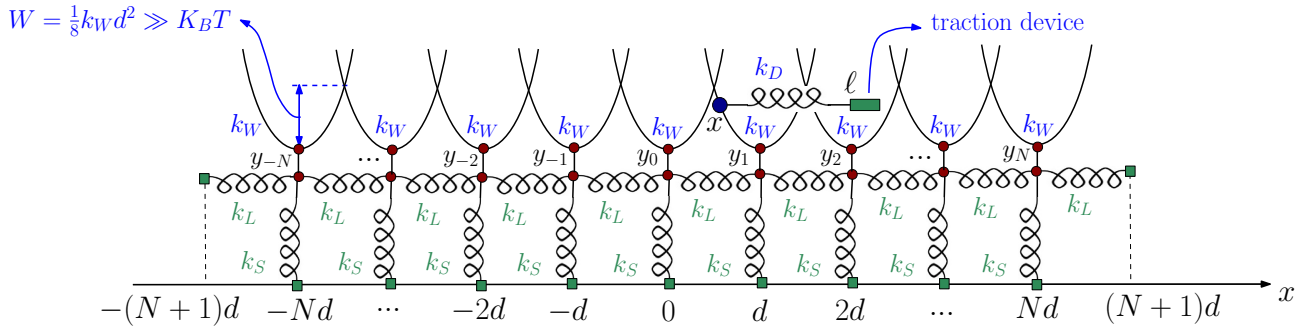

Fig. 1 Scheme of the soft corrugated substrate with a moving slider placed at x, pulled by a traction device placed at ℓ and with an intrinsic stiffness k_D. The deformable substrate is composed of a sequence of quadratic energy potential wells with stiffness k_W and separated by an energy barrier $W = k_W d^2/8 \gg K_B T$. The positions of the centers of these potential wells are identified by the variables y_j with $-N \leq j \leq +N$, which can be shifted with respect to their equilibrium positions jd for $-N \leq j \leq +N$, being d the lattice constant of the substrate. The deformability of the substrate is controlled by an elastic ladder network composed of longitudinal springs k_L and shear springs k_S. As an example, in this plot the slider is placed within the well centered in y_1 and therefore we have the value $s = 1$ for the discrete spin variable.

collective motion of cells. Understanding this phenomenon is essential to elucidate the mechanisms involved in wound healing, cancerous metastases evolution, and tissues development.[36,37] These processes are extremely complex and therefore knowing the effects of the substrate stiffness in an oversimplified configuration can help to understand the contribution of the many factors involved in the real problems (intracellular adhesion and signaling, cell polarization, and so on). It is first important to note that the movement of cells on a substrate is actually characterized by stick-slip motion, as recently observed.[38–40] Then, frictional phenomena between cells and substrate are essential to regulate cells motion and related mechanosensitive processes.[41] It has been observed that isolated cells exhibit a direction of migration aligned with the gradient of the substrate stiffness (durotaxis),[42–44] and groups of interacting cells also follow the same principle (collective durotaxis).[45] This is consistent with the fact that the traction force increases with the stiffness of the substrate.[41,46] Correspondingly, evidence has been provided that the friction experienced by cells is an increasing function of substrate stiffness.[47–49] Interestingly, this observation is in perfect agreement with the results obtained by means of the model here proposed for the stick-slip phenomenon on soft substrate, as discussed below. Anyway, a complete view on the motion of cells is not yet available, and many points remain to be clarified: cells propagate faster with increasing stiffness only up to optimal stiffness,[50] there are different cells migration modes to investigate,[51] wrinkles appear in bacterial biofilms growing on soft substrates,[52] and the cells motion shows a biphasic relation with substrate stiffness and friction.[53] It is interesting to remember that, from the experimental point of view, ad-hoc soft substrates are used to measure the field of forces applied on the substrate itself by cells. This is done through the so-called Traction Force Microscopy[54], which is particularly useful to correlate the mechanical features of cancer cells to metastatic phenomena, which are, in turn, strongly influenced by temperature.[55] The stick-slip phenomenon is also artificially induced in several bioinspired micro- and nano-structured materials in order to mimic, for example, the remarkable mechanical properties of gecko's feet.[56–58] At a larger scale, stick-slip and wear are largely studied, by means of the Surface Forces Apparatus,[15] in articular cartilage, with the aim of detecting and tracking the progression of articular joints diseases.[59] These approaches proved that prolonged stick-slip sliding of cartilage can increase the surface roughness, eventually inducing damage.[60] Although our model is extremely simple with respect to these complex systems, it represents a first step in modeling thermal effects on friction phenomena with soft substrates and can provide the first general insights into stick-slip behavior in these structures. Of course, in the near future it can be generalized to take into account all the more realistic elements that are neglected here.

In a rather different field of study, the modeling of the stick-slip processes on soft substrate is important to better understand the friction behavior on artificial elastomeric wrinkled or micropatterned surfaces with applications to haptic technologies, augmented reality and tactile robotics.[61–65]

The proposed model is based on equilibrium statistical mechanics and it is implemented by means of the spin variable approach, useful to deal with arbitrarily nonconvex potential energies.[66] This method has been largely applied to several situations including the physics of muscles,[67,68] the folding of macromolecules,[69–73] the adhesion/deadhesion processes,[74,75] the phase transformations in solids,[76,77] and the stick-slip on rigid substrate.[78] Essentially, this technique made it possible to complement the methods typically used to study the behavior of physical systems with multiple stable and metastable states.[79–82] In this study, we consider a moving slider in contact with a substrate described by a sequence of elastically bound quadratic energy wells (see Fig.1). The spin variables approach is particularly useful since allows a direct calculation of the partition function for our system with soft substrate. We can therefore efficiently determine all thermodynamic variables of interest (when the energy barrier between the wells is sufficiently larger than $K_B T$). The method is based on the introduction of a discrete or spin variable, able to identify the energy well explored by the sliding particle. Firstly, a finite length substrate is considered and the statistical behavior of the system is investigated. Then, the obtained results have been simplified from the mathematical point of view, enabling an efficient implementation of the model. The underly-

ing physics has been taken into consideration by discussing the average spin variable (average position of the slider), the average stick-slip or static friction force, the average substrate deformation, and the probability density of the variable slider position. These quantities have been studied for a variable temperature and substrate stiffness. To conclude, the limiting case of an infinitely long soft substrate has been analyzed, eventually obtaining closed form expressions for all relevant thermodynamic quantities. Interestingly, these expressions were written in terms of a Jacoby's Theta function. The most striking results represent the increase in stick-slip force with substrate stiffness (relevant for the cells motion understanding), and its decrease with temperature (relevant for thermolubricity applications).

The paper is organized as follows. In Section 2, we introduce the thermal model for the stick-slip phenomenon on soft substrate. Then, in Section 3, we describe a mathematical simplification allowing for an efficient implementation of the model. We discuss here the physics underlyng the behavior of the system. In the following Section 4, we perform the limit of the theory with an infinite long substrate. Finally, the Conclusions and two Appendixes close the manuscript.

2 Thermal model for stick-slip on soft substrate

We consider a particle identified with the position x, sliding over a one-dimensional soft or deformable corrugated substrate (see Fig.1). This substrate is characterized by a sequence of quadratic potential wells centered at positions y_j with $-N \leq j \leq +N$, and having an elastic coefficient equal to k_W. When the substrate is in equilibrium, i.e. there is no action of the sliding particle, the wells centers are equispaced (on the x-axis) with $y_j = jd$ for $-N \leq j \leq +N$, being d the lattice constant of the substrate. In this condition, we have the energy barrier $W = k_W d^2/8$ between adjacent wells. This is reminiscent of the periodic substrate of the Prandtl-Tomlinson model[19–22]. However, when the particle slides on the substrate, the wells centers y_j show a displacement $y_j - jd \neq 0$ induced by the interaction between slider and substrate. The soft substrate is modeled by means of a springs ladder network composed of longitudinal springs of elastic constant k_L and shear springs with elastic constant k_S (see Fig.1). It means that a spring k_L (with equilibrium length d) links all pairs of adjacent wells centers, placed at y_j and y_{j-1}. Moreover, each well center at y_j is linked to the fixed position jd through a spring k_S (with zero equilibrium length). While k_L controls the spatial extent of the displacement perturbation as the particle slides on the substrate, k_S controls the stiffness of the substrate itself. In addition, the particle is moved by a traction device placed at position ℓ (which is variable) and with elastic constant k_D. Eventually, the total potential energy of the system can be written as

$$\begin{aligned} U(x,s,\vec{y}) &= \frac{1}{2}k_W(x-y_s)^2 + \frac{1}{2}k_D(\ell-x)^2 \\ &+ \frac{1}{2}k_L\sum_{j=-N+1}^{+N}(y_j-y_{j-1}-d)^2 + \frac{1}{2}k_S\sum_{j=-N}^{+N}(y_j-jd)^2 \\ &+ \frac{1}{2}k_L(y_{-N}+Nd)^2 + \frac{1}{2}k_L(Nd-y_{+N})^2, \end{aligned} \tag{1}$$

where the discrete or spin variable $-N \leq s \leq +N$ represents the potential well explored by the slider and $\vec{y}$ is the vector of wells centers positions $y_{-N},...,y_{+N}$. The last two terms represent the energy contributions of the two outermost longitudinal springs k_L that connect y_{-N} with the fixed position $-(N+1)d$, and y_{+N} with the fixed position $(N+1)d$. Here, the elastic springs are named following the identifications: W→well, D→device, L→longitudinal, and S→shear.

We suppose that the system is in contact with a thermal bath at temperature T and that the velocity of the sliding particle is low enough to be able to neglect dynamical effects. It means that we study the thermal behavior of the static or quasi-static stick-slip phenomenon on a soft substrate. To approach the problem, we can therefore apply the equilibrium statistical mechanics characterized by the classical canonical distribution. In order to calculate the corresponding partition function, we can sum over the spins variables and integrate over the continuous variables independently. This allows the partition function to be written in the following form

$$Z = \sum_{s=-N}^{+N}\int_{\mathbb{R}^{2N+1}}\int_{-\infty}^{+\infty} e^{-\frac{U(x,s,\vec{y})}{K_BT}}\,\mathrm{d}x\mathrm{d}\vec{y}, \tag{2}$$

where K_B is the Boltzmann constant and T is the temperature. Of course, the application of the spins method introduces an approximation and therefore there are physical limitations to the use of the model. In fact, each continuous variable is integrated over the whole span of real values and not only over the range it would be allowed in the exact model. This introduces an error in the regions where the tails of the Gaussian functions overlap. However, this error is negligible when the energy barrier W between the elastic substrate wells is sufficiently larger than the thermal energy K_BT. This means that we are led to assume that $W = k_W d^2/8 \gg K_BT$.

The partition function defined in Eq.(2) can be elaborated as follows, by first performing the integral on x and then on $\vec{y}$. To begin with, in order to separate the terms depending on x from the others, the total energy U can be rewritten as follows

$$U(x,s,\vec{y}) = \frac{1}{2}(k_W+k_D)x^2 - (k_W y_s + k_D\ell)x + \Theta(s,\vec{y}), \tag{3}$$

where Θ is independent of x and reads

$$\begin{aligned} \Theta(s,\vec{y}) &= \frac{1}{2}k_W y_s^2 + \frac{1}{2}k_D\ell^2 \\ &+ \frac{1}{2}k_L\sum_{j=-N}^{N}(y_j-y_{j-1}-d)^2 + \frac{1}{2}k_S\sum_{j=-N}^{N}(y_j-jd)^2 \\ &+ \frac{1}{2}k_L(y_{-N}+Nd)^2 + \frac{1}{2}k_L(Nd-y_{+N})^2. \end{aligned} \tag{4}$$

Hence, this separation allows to write the partition function in the form

$$Z = \sum_{s=-N}^{+N}\int_{\mathbb{R}^{2N+1}} e^{-\frac{\Theta(s,\vec{y})}{K_BT}}\int_{-\infty}^{+\infty} e^{-\frac{k_W+k_D}{2K_BT}x^2 + \frac{k_W y_s + k_D\ell}{K_BT}x}\mathrm{d}x\mathrm{d}\vec{y}, \tag{5}$$

where the integration over x can be performed in closed form by

means of the well-known expression

$$\int_{-\infty}^{+\infty} e^{-\alpha x^2} e^{\beta x} dx = \sqrt{\frac{\pi}{\alpha}} e^{\frac{\beta^2}{4\alpha}} \quad (\alpha > 0). \tag{6}$$

Then, we get

$$\begin{aligned} Z &= \sqrt{\frac{2\pi K_B T}{k_W + k_D}} \sum_{s=-N}^{+N} \int_{\mathbb{R}^{2N+1}} e^{-\frac{\Theta(s,\vec{y})}{K_B T}} e^{\frac{(k_W y_s + k_D \ell)^2}{2(k_W+k_D)K_B T}} \mathrm{d}\vec{y} \\ &= \sqrt{\frac{2\pi K_B T}{k_W + k_D}} \sum_{s=-N}^{+N} \int_{\mathbb{R}^{2N+1}} e^{-\frac{\Omega(s,\vec{y})}{K_B T}} \mathrm{d}\vec{y}, \end{aligned} \tag{7}$$

where we introduced the quantity

$$\Omega(s,\vec{y}) = \Theta(s,\vec{y}) - \frac{(k_W y_s + k_D \ell)^2}{2(k_W + k_D)}. \tag{8}$$

This is a quadratic function in the variable $\vec{y}$ that can be developed by means of a long but straightforward calculation based on Eq.(4). The result is

$$\begin{aligned} \Omega(s,\vec{y}) &= \frac{1}{2}\ell^2 \frac{k_W k_D}{k_W + k_D} + N(N+1)k_L d^2 + \frac{1}{6}N(N+1)(2N+1)k_S d^2 \\ &+ k_L \ell \vec{\xi}_s \cdot \vec{y} + \frac{1}{2} k_L \vec{y} \cdot \mathscr{A}_s \vec{y}, \end{aligned} \tag{9}$$

where we used the relation $\sum_{j=-N}^{+N} j^2 = N(N+1)(2N+1)/3$. In this expression, the tridiagonal matrix $\mathscr{A}_s$ is defined as

$$\mathscr{A}_s = \begin{bmatrix} a_{-N} & -1 & 0 & \dots & 0 \\ -1 & a_{-N+1} & -1 & \ddots & \vdots \\ 0 & -1 & \ddots & \ddots & 0 \\ \vdots & \ddots & \ddots & a_{N-1} & -1 \\ 0 & \dots & 0 & -1 & a_N \end{bmatrix} \in \mathscr{M}_{2N+1,2N+1}(\mathbb{R}), \tag{10}$$

with all the subdiagonal and superdiagonal elements equal to -1 and the diagonal elements given by

$$a_j = 2 + \frac{k_S}{k_L} + \delta_{j,s} \frac{k_W k_D}{k_L (k_W + k_D)}, \tag{11}$$

with $-N \leq j \leq +N$, $-N \leq s \leq +N$, and where $\delta_{a,b}$ is the Kronecker delta, assuming the value 1 when $a = b$, and the value zero when $a \neq b$. It means that the term $\frac{k_W k_D}{k_L(k_W+k_D)}$ is added to the element a_s of the diagonal of $\mathscr{A}_s$. In particular, if $s = -N$, it is added to the first element and, if $s = +N$, to the last one. This means that the matrix $\mathscr{A}_s$ is dependent on s since this term shifts as s varies. Moreover, the vector $\vec{\xi}_s \in \mathbb{R}^{2N+1}$ in Eq.(9) is defined as

$$\vec{\xi}_s = (\xi_{s,-N}, \xi_{s,-N+1}, ..., \xi_{s,N-1}, \xi_{s,N}), \tag{12}$$

where

$$\xi_{s,j} = \frac{(N+1)d}{\ell} \left(\delta_{j,-N} - \delta_{j,+N}\right) - j\frac{d}{\ell}\frac{k_S}{k_L} - \delta_{j,s} \frac{k_W k_D}{k_L (k_W + k_D)}, \tag{13}$$

again with $-N \leq j \leq +N$, $-N \leq s \leq +N$. In this case, the term $\frac{k_W k_D}{k_L(k_W+k_D)}$ is subtracted from the element $\xi_{s,s}$ of the vector $\vec{\xi}_s$. Again, the vector $\vec{\xi}_s$ depends on s because of the shift of this term as s varies.

At the end of this development, we observe that $\Omega(s,\vec{y})$ is written in Eq.(9) as a quadratic function in the vector $\vec{y}$, composed of three contributions: a constant term with respect to $\vec{y}$ (first line of Eq.(9)), a term of first degree in $\vec{y}$ (controlled by the vector $\vec{\xi}_s$), and a term of second degree in $\vec{y}$ (controlled by the matrix $\mathscr{A}_s$). We can substitute this expression of $\Omega(s,\vec{y})$ into the partition function defined in Eq.(7). Importantly, the integral can now be performed by using the gaussian property

$$\int_{\mathbb{R}^M} e^{-\frac{1}{2}\vec{y}\cdot\mathscr{B}\vec{y}} e^{\vec{b}\cdot\vec{y}} d\vec{y} = \sqrt{\frac{(2\pi)^M}{\det \mathscr{B}}} e^{\frac{1}{2}\vec{b}\cdot\mathscr{B}^{-1}\vec{b}}, \tag{14}$$

holding for any symmetric and positive definite matrix $\mathscr{B} \in \mathscr{M}_{M,M}(\mathbb{R})$ and for any vector $\vec{b} \in \mathbb{R}^M$. The explicit form of the partition function is then delivered as follows

$$\begin{aligned} Z &= \sqrt{\frac{(2\pi K_B T)^{2N+2}}{(k_W + k_D) k_L^{2N+1}}} e^{-\frac{N(N+1)k_L d^2}{K_B T}} e^{-\frac{N(N+1)(2N+1)k_S d^2}{6K_B T}} \\ &\times \sum_{s=-N}^{+N} \frac{1}{\sqrt{\det \mathscr{A}_s}} e^{\frac{k_L \ell^2}{2K_B T}\left[\vec{\xi}_s \cdot \mathscr{A}_s^{-1} \vec{\xi}_s - \frac{k_W k_D}{k_L(k_W+k_D)}\right]}. \end{aligned} \tag{15}$$

Therefore, the joint probability density of all the variables belonging to the phase space of the system is readily written in the canonical form

$$\rho(x,s,\vec{y}) = \frac{1}{Z} e^{-\frac{U(x,s,\vec{y})}{K_B T}}, \tag{16}$$

with the normalization property

$$\sum_{s=-N}^{+N} \int_{\mathbb{R}^{2N+1}} \int_{-\infty}^{+\infty} \rho(x,s,\vec{y}) \mathrm{d}x \mathrm{d}\vec{y} = 1. \tag{17}$$

In particular, the knowledge of the partition function allows us to obtain the average value of the static or quasi-static friction force, or stick-slip force, by means of the thermodynamic relation

$$\langle f \rangle = -K_B T \frac{\partial \log Z}{\partial \ell} = -K_B T \frac{1}{Z} \frac{\partial Z}{\partial \ell}. \tag{18}$$

This is true within the Helmholtz statistical ensemble of the statistical mechanics.[83,84] Moreover, this can be easily seen by deriving Z in Eq.(2) with respect to ℓ, by considering the total energy in Eq.(1), and by observing that $\langle f \rangle = k_D(\ell - \langle x \rangle)$. A straightforward development of the derivative yields the following explicit result

$$\langle f \rangle = \ell \frac{k_W k_D}{k_W + k_D} \frac{\displaystyle\sum_{s=-N}^{+N} \frac{1}{\sqrt{\det \mathscr{A}_s}} e^{\frac{k_L \ell^2}{2K_B T} \vec{\xi}_s \cdot \mathscr{A}_s^{-1} \vec{\xi}_s} \left(1 + \vec{e}_s \cdot \mathscr{A}_s^{-1} \vec{\xi}_s\right)}{\displaystyle\sum_{s=-N}^{+N} \frac{1}{\sqrt{\det \mathscr{A}_s}} e^{\frac{k_L \ell^2}{2K_B T} \vec{\xi}_s \cdot \mathscr{A}_s^{-1} \vec{\xi}_s}}, \tag{19}$$

where $\vec{e}_s$ is the $(s+N+1)$-th element of the canonical basis of the space $\mathbb{R}^{2N+1}$, i.e. $\vec{e}_s = (0,0,...,1,...,0,0)$ where the one is at position $s+N+1$ with $-N \leq s \leq +N$. Importantly, this value of the rate-independent stick-slip force takes into consideration the deformation of the substrate and indeed depends on the elastic properties of the substrate itself. We will thoroughly explore the effect of the substrate deformability on the rate-independent

stick-slip force force. Of course, since $\langle f\rangle = k_D(\ell - \langle x\rangle)$, the knowledge of $\langle f\rangle$ also makes it easy to determine the value of $\langle x\rangle$. We do not report formulas and graphs for $\langle x\rangle$ so as not to lengthen the article further.

Another important macroscopic observable is given by the average value of the spin variable s. It has a similar meaning as $\langle x\rangle$ but allows for better identification of jumps between wells. It can be simply determined through the following expression, directly derived from the probability density in Eq.(16)

$$\langle s\rangle = \sum_{s=-N}^{+N} s \int_{\mathbb{R}^{2N+1}} \int_{-\infty}^{+\infty} \rho(x,s,\vec{y})\mathrm{d}x\mathrm{d}\vec{y}. \tag{20}$$

A not difficult elaboration leads to the explicit result

$$\langle s\rangle = \frac{\sum_{s=-N}^{+N} \frac{s}{\sqrt{\det \mathscr{A}_s}} e^{\frac{k_L\ell^2}{2K_BT}\vec{\xi}_s\cdot\mathscr{A}_s^{-1}\vec{\xi}_s}}{\sum_{s=-N}^{+N} \frac{1}{\sqrt{\det \mathscr{A}_s}} e^{\frac{k_L\ell^2}{2K_BT}\vec{\xi}_s\cdot\mathscr{A}_s^{-1}\vec{\xi}_s}}, \tag{21}$$

representing the average value of the discrete variable identifying the energy well locally explored by the moving slider. It is useful to determine the average number $\langle s\rangle$ corresponding to the energy well in which the slider is located in terms of the position ℓ of the traction device.

The most original quantity obtained in this work represents the deformation induced in the corrugated substrate by the sliding particle. It is quantified by the average value of position vector $\vec{y}$, which can be calculated as

$$\langle \vec{y}\rangle = \sum_{s=-N}^{+N} \int_{\mathbb{R}^{2N+1}} \int_{-\infty}^{+\infty} \rho(x,s,\vec{y})\vec{y}\mathrm{d}x\mathrm{d}\vec{y}. \tag{22}$$

The integration can be performed by means of a generalization of Eq.(14), given by

$$\int_{\mathbb{R}^M} e^{-\frac{1}{2}\vec{y}\cdot\mathscr{B}\vec{y}} e^{\vec{b}\cdot\vec{y}}\vec{y}d\vec{y} = \sqrt{\frac{(2\pi)^M}{\det\mathscr{B}}} e^{\frac{1}{2}\vec{b}\cdot\mathscr{B}^{-1}\vec{b}}\mathscr{B}^{-1}\vec{b}, \tag{23}$$

holding again for any symmetric and positive definite matrix $\mathscr{B} \in \mathscr{M}_{M,M}(\mathbb{R})$ and for any vector $\vec{b} \in \mathbb{R}^M$. With the application of Eq.(23), the definition in Eq.(22) eventually delivers the explicit expression

$$\langle \vec{y}\rangle = -\ell \frac{\sum_{s=-N}^{+N} \frac{1}{\sqrt{\det \mathscr{A}_s}} e^{\frac{k_L\ell^2}{2K_BT}\vec{\xi}_s\cdot\mathscr{A}_s^{-1}\vec{\xi}_s}\mathscr{A}_s^{-1}\vec{\xi}_s}{\sum_{s=-N}^{+N} \frac{1}{\sqrt{\det \mathscr{A}_s}} e^{\frac{k_L\ell^2}{2K_BT}\vec{\xi}_s\cdot\mathscr{A}_s^{-1}\vec{\xi}_s}}. \tag{24}$$

This result represents the positions (on the x-axis) of the centers of the energy wells (constituting the deformable substrate) as function of the position ℓ of the moving slider.

An additional quantity, which will be useful to better understand the behavior of the system, consists in the probability density $\rho(x)$ of the single variable x. Of course, it is defined as

$$\rho(x) = \sum_{s=-N}^{+N} \int_{\mathbb{R}^{2N+1}} \rho(x,s,\vec{y})\mathrm{d}\vec{y} = \frac{1}{Z}\sum_{s=-N}^{+N} \int_{\mathbb{R}^{2N+1}} e^{-\frac{U(x,s,\vec{y})}{K_BT}}\mathrm{d}\vec{y}, \tag{25}$$

and it is subjected to the normalization condition

$$\int_{-\infty}^{+\infty} \rho(x)\mathrm{d}x = 1. \tag{26}$$

We use the same symbol for $\rho(x)$ and for $\rho(x,s,\vec{y})$ but always indicate the variables to avoid any ambiguity. In order to perform the calculation of $\rho(x)$, we need to rewrite the total energy U by identifying the terms independent of $\vec{y}$, and those representing a quadratic function in $\vec{y}$. So doing, we obtain the expression

$$\begin{aligned} U(x,s,\vec{y}) &= \frac{1}{2}k_W x^2 + \frac{1}{2}k_D x^2 - k_D\ell x + \frac{1}{2}k_D\ell^2 \\ &+ N(N+1)k_L d^2 + \frac{1}{6}N(N+1)(2N+1)k_S d^2 \\ &+ \frac{1}{2}k_L\vec{y}\cdot\mathscr{C}_s\vec{y} + k_L\ell\vec{\zeta}_s\cdot\vec{y}, \end{aligned} \tag{27}$$

where the last two terms represent the second order contribution in $\vec{y}$ (controlled by $\mathscr{C}_s \in \mathscr{M}_{2N+1,2N+1}(\mathbb{R})$) and the first order contribution (controlled by $\vec{\zeta}_s \in \mathbb{R}^{2N+1}$). Here, the tridiagonal matrix $\mathscr{C}_s$ is given by

$$\mathscr{C}_s = \begin{bmatrix} c_{-N} & -1 & 0 & \dots & 0 \\ -1 & c_{-N+1} & -1 & \ddots & \vdots \\ 0 & -1 & \ddots & \ddots & 0 \\ \vdots & \ddots & \ddots & c_{N-1} & -1 \\ 0 & \dots & 0 & -1 & c_N \end{bmatrix} \in \mathscr{M}_{2N+1,2N+1}(\mathbb{R}), \tag{28}$$

with all the subdiagonal and superdiagonal elements equal to -1 and the diagonal elements given by

$$c_j = 2 + \frac{k_S}{k_L} + \delta_{j,s}\frac{k_W}{k_L}. \tag{29}$$

The last term in Eq.(29) means that the quantity $\frac{k_W}{k_L}$ is added only to the element c_s of the main diagonal of $\mathscr{C}_s$. Similarly, we find that the vector $\vec{\zeta}_s$ is defined as

$$\vec{\zeta}_s = (\zeta_{s,-N}, \zeta_{s,-N+1}, \dots, \zeta_{s,N-1}, \zeta_{s,N}), \tag{30}$$

where one must consider the following components

$$\zeta_{s,j} = \frac{(N+1)d}{\ell}\left(\delta_{j,-N} - \delta_{j,+N}\right) - j\frac{d}{\ell}\frac{k_S}{k_L} - \delta_{j,s}\frac{k_W}{k_L}\frac{x}{\ell}, \tag{31}$$

always with $-N \le j \le +N$, $-N \le s \le +N$. As before, the last term means that the quantity $\frac{k_W}{k_L}\frac{x}{\ell}$ is subtracted only from the element $\zeta_{s,s}$ of the vector $\vec{\zeta}_s$. To conclude, the substitution of the total energy written as in Eq.(27) into Eq.(25), and the application of the property stated in Eq.(14), yields the probability density $\rho(x)$ in the form

$$\rho(x) = \frac{e^{-\frac{k_W+k_D}{2K_BT}\left(x-\frac{k_D\ell}{k_W+k_D}\right)^2}\sum_{s=-N}^{+N}\frac{1}{\sqrt{\det\mathscr{C}_s}}e^{\frac{k_L\ell^2}{2K_BT}\vec{\zeta}_s\cdot\mathscr{C}_s^{-1}\vec{\zeta}_s}}{\sqrt{\frac{2\pi K_BT}{k_W+k_D}}\sum_{s=-N}^{+N}\frac{1}{\sqrt{\det\mathscr{A}_s}}e^{\frac{k_L\ell^2}{2K_BT}\vec{\xi}_s\cdot\mathscr{A}_s^{-1}\vec{\xi}_s}}, \tag{32}$$

where all the quantities $\mathscr{A}_s$, $\vec{\xi}_s$, $\mathscr{C}_s$, and $\vec{\zeta}_s$ have been previously

defined, see Eqs.(10),(13),(28), and (31). It is possible to prove that the obtained form for $\rho(x)$ in Eq.(32) exactly satisfies the normalization condition in Eq.(26). This concludes the mathematical analysis of the system. We obtained the average stick-slip force in Eq.(19), the expectation value of the spin variable in Eq.(21), the average value of the substrate displacement in Eq.(24), and the density of probability of x in Eq.(32). However, it is important to remark that the sums indicated in all these results are quite costly from the numerical point of view since we need to determine the determinant and the inverse matrix of $\mathscr{A}_s$ and $\mathscr{C}_s$ for any value of s in the range $-N \leq s \leq +N$. If the number $2N+1$ of binding sites of the corrugated substrate is large, the procedure is rather demanding especially if we are interested in performing a parametric analysis of the system behavior. For this reason, we show in the next Section a further simplification of these results, based on specific matrix properties.

3 Efficient implementation of the model

All results obtained in the previous Section can be further simplified (without approximations) in view of an efficient numerical implementation. To this aim, we can prove the two following mathematical properties. First of all, we define the Kronecker product of two vectors $\vec{v} \in \mathbb{R}^M$ and $\vec{w} \in \mathbb{R}^M$ such that $\vec{v} \otimes \vec{w} \in \mathscr{M}_{M,M}(\mathbb{R})$ and $(\vec{v} \otimes \vec{w})_{ij} = v_i w_j$. Then, we introduce a matrix $\mathscr{B} \in \mathscr{M}_{M,M}(\mathbb{R})$ and a vector $\vec{b} \in \mathbb{R}^M$ such that $\mathscr{B}^{-1}$ and $\left(\mathscr{B} + x\vec{b} \otimes \vec{b}\right)^{-1}$ exist for some $x \in \mathbb{R}$. Under these assumptions, the two following relations can be proved (see Appendix A)

$$\left(\mathscr{B} + x\vec{b} \otimes \vec{b}\right)^{-1} = \mathscr{B}^{-1} - x\frac{\mathscr{B}^{-1}\vec{b} \otimes \vec{b}\mathscr{B}^{-1}}{1 + x\vec{b} \cdot \mathscr{B}^{-1}\vec{b}}, \quad (33)$$

$$\det\left(\mathscr{B} + x\vec{b} \otimes \vec{b}\right) = \det\mathscr{B}\left(1 + x\vec{b} \cdot \mathscr{B}^{-1}\vec{b}\right). \quad (34)$$

These results allow the determination of the inverse and the determinant of $\mathscr{B} + x\vec{b} \otimes \vec{b}$ by means of the calculation of $\mathscr{B}^{-1}$ and $\det\mathscr{B}$. So, $\mathscr{B}^{-1}$ and $\det\mathscr{B}$ can be calculated once and for all regardless of the value of x. Interestingly, these properties can be directly applied to our previous formulas by observing that

$$\mathscr{A}_s = \mathscr{N} + \alpha\gamma\vec{e}_s \otimes \vec{e}_s, \quad (35)$$

$$\mathscr{C}_s = \mathscr{N} + \alpha\vec{e}_s \otimes \vec{e}_s, \quad (36)$$

$$\vec{\xi}_s = \vec{\eta} - \alpha\gamma\vec{e}_s, \quad (37)$$

$$\vec{\zeta}_s = \vec{\eta} - \alpha\vec{e}_s\frac{x}{\ell}, \quad (38)$$

$$\gamma = \frac{k_D}{k_W + k_D}, \quad (39)$$

$$\alpha = \frac{k_W}{k_L}. \quad (40)$$

For the sake of clarity, we underline that Eq.(35) comes from Eqs.(10) and (11), Eq.(36) comes from Eqs.(28) and (29), Eq.(37) comes from Eqs.(12) and (13), and finally Eq.(38) comes from Eqs.(30) and (31). Here, the matrix $\mathscr{N}$ is defined as

$$\mathscr{N} = \begin{bmatrix} n_{-N} & -1 & 0 & \dots & 0 \\ -1 & n_{-N+1} & -1 & \ddots & \vdots \\ 0 & -1 & \ddots & \ddots & 0 \\ \vdots & \ddots & \ddots & n_{N-1} & -1 \\ 0 & \dots & 0 & -1 & n_N \end{bmatrix} \in \mathscr{M}_{2N+1,2N+1}(\mathbb{R}), \quad (41)$$

with all the subdiagonal and superdiagonal elements equal to -1 and the diagonal elements given by

$$n_j = 2 + \frac{k_S}{k_L} = 2 + \lambda \ \ \forall j, \quad (42)$$

where $\lambda = k_S/k_L$. Hence, $\mathscr{N}$ is a tridiagonal matrix with all elements on the main diagonal assuming the same value $2 + k_S/k_L = 2 + \lambda$. Moreover, the vector $\vec{\eta}$ is defined as

$$\vec{\eta} = (\eta_{-N}, \eta_{-N+1}, ..., \eta_{N-1}, \eta_N), \quad (43)$$

and has the following components

$$\eta_j = \frac{(N+1)d}{\ell}\left(\delta_{j,-N} - \delta_{j,+N}\right) - j\frac{d}{\ell}\frac{k_S}{k_L}. \quad (44)$$

for $-N \leq j \leq +N$. The important result is that neither $\mathscr{N}$ nor $\vec{\eta}$ are dependent on s. Then we can use Eqs.(33) and (34) in order to further elaborate the main results of the previous Section. A straightforward algebraic development yields the following expressions

$$\vec{\xi}_s \cdot \mathscr{A}_s^{-1}\vec{\xi}_s = \vec{\eta} \cdot \mathscr{N}^{-1}\vec{\eta} + \alpha\gamma - \alpha\gamma\frac{(1+z_s)^2}{1 + \alpha\gamma\mathscr{N}_{ss}^{-1}}, \quad (45)$$

$$\mathscr{A}_s^{-1}\vec{\xi}_s = \mathscr{N}^{-1}\vec{\eta} - \alpha\gamma\mathscr{N}^{-1}\vec{e}_s\frac{1+z_s}{1 + \alpha\gamma\mathscr{N}_{ss}^{-1}}, \quad (46)$$

$$1 + \vec{e}_s \cdot \mathscr{A}_s^{-1}\vec{\xi}_s = \frac{1+z_s}{1 + \alpha\gamma\mathscr{N}_{ss}^{-1}}, \quad (47)$$

$$\vec{\zeta}_s \cdot \mathscr{C}_s^{-1}\vec{\zeta}_s = \vec{\eta} \cdot \mathscr{N}^{-1}\vec{\eta} + \alpha\frac{x^2}{\ell^2} - \alpha\frac{\left(\frac{x}{\ell} + z_s\right)^2}{1 + \alpha\mathscr{N}_{ss}^{-1}}, \quad (48)$$

$$\det\mathscr{A}_s = \det\mathscr{N}\left(1 + \alpha\gamma\mathscr{N}_{ss}^{-1}\right), \quad (49)$$

$$\det\mathscr{C}_s = \det\mathscr{N}\left(1 + \alpha\mathscr{N}_{ss}^{-1}\right), \quad (50)$$

where $\mathscr{N}_{ss}^{-1} = \vec{e}_s \cdot \mathscr{N}^{-1}\vec{e}_s$, i.e. it is the $(s+N+1)$-th element on the main diagonal of the matrix $\mathscr{N}^{-1}$, and $z_s = \vec{e}_s \cdot \mathscr{N}^{-1}\vec{\eta}$. We remember that $\vec{e}_s$ is the $(s+N+1)$-th element of the canonical basis of the space $\mathbb{R}^{2N+1}$, i.e. $\vec{e}_s = (0,0,...,1,...,0,0)$ where the one is at position $s+N+1$ with $-N \leq s \leq +N$. In conclusion, these expressions, easily derived by the properties in Eqs.(33) and (34), allow us to implement all results obtained in previous Section by calculating only one inverse matrix, namely of $\mathscr{N} \in \mathscr{M}_{2N+1,2N+1}(\mathbb{R})$.

All these results can be written by introducing the following

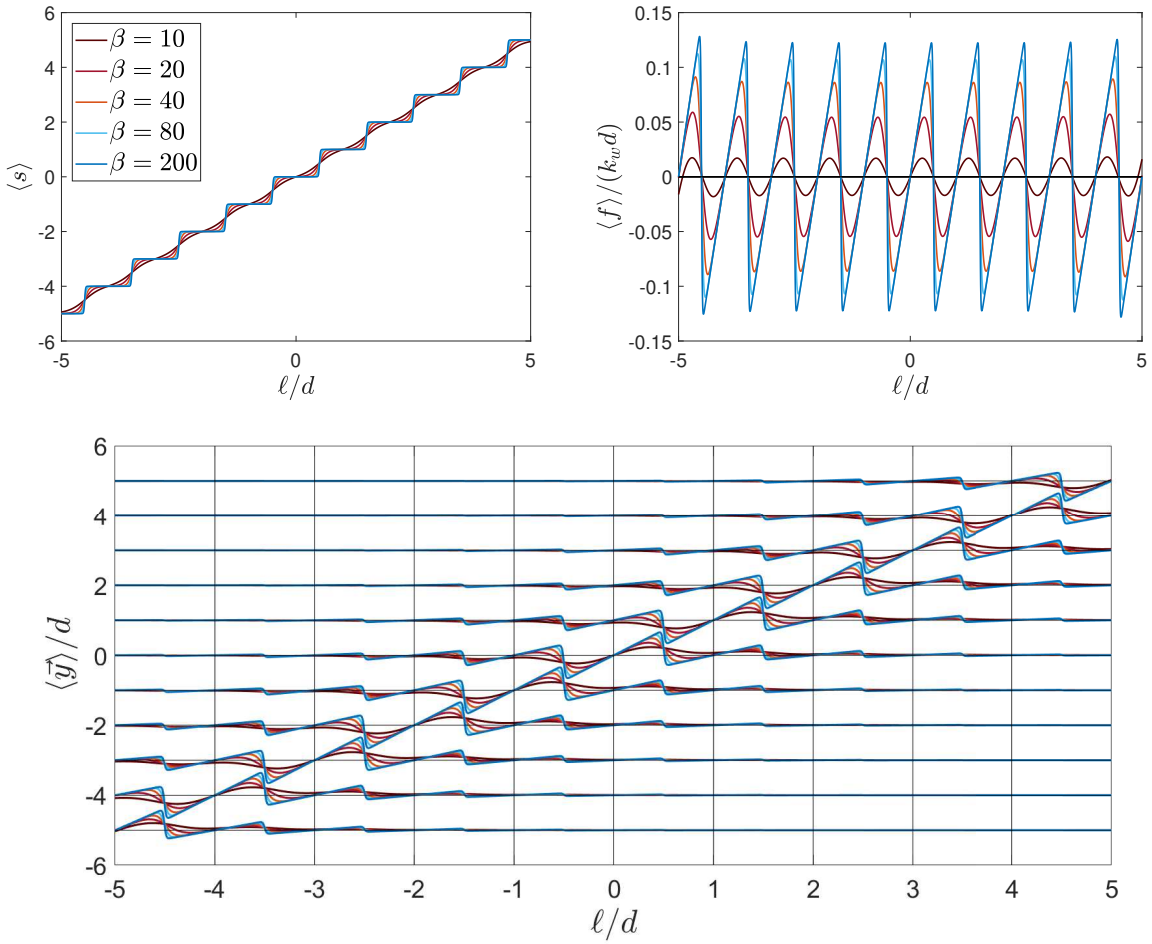

Fig. 2 Effect of the temperature on the stick-slip process. We show the average value of the spin variable $\langle s \rangle$, the average value of the normalized stick-slip force $\langle f \rangle/(k_w d)$, and the substrate positions vector $\langle \vec{y} \rangle/d$ as function of ℓ/d for a chain with $N = 5$ and for different values of β. We adopted the parameters $k_L = 4$, $k_S = 3$, $k_W = 8$, $k_D = 5$, $d = 1$, $K_B T = 2/5, 1/5, 1/10, 1/20, 1/50$ in arbitrary units, corresponding to the following adimensional quantities: $\gamma = 5/13$, $\lambda = 3/4$, $\alpha = 2$, $\beta = 10, 20, 40, 80, 200$. In order to better visualize the behavior of the normalized positions $\langle y_j \rangle/d$, $-N \leq j \leq +N$, we plotted the curves $(\langle y_j \rangle/d - j)\mathscr{A} + j$, $-N \leq j \leq +N$, where we adopted the amplification factor $\mathscr{A} = 5$.

parameter

$$\beta = \frac{k_W d^2}{2K_B T}, \tag{51}$$

which perfectly describes the compromise between the depth of the energy wells of the soft corrugated substrate and the thermal fluctuations. For the spin variable approach considered to work properly, the barrier $W = k_W d^2/8$ between two adjacent wells must be sufficiently larger than the thermal energy $K_B T$, as previously discussed. It means that we will consider $\beta \gg 4$. Anyway, the previous results can be rewritten in a more effective form. Concerning the rate-independent stick-slip force, from Eq.(19), we get

$$\frac{\langle f \rangle}{k_w d} = \frac{\ell}{d} \frac{\sum_{s=-N}^{+N} \frac{\gamma(1+z_s)}{\left(1+\alpha\gamma\mathscr{N}_{ss}^{-1}\right)^{3/2}} e^{-\beta\gamma\frac{\ell^2}{d^2}\frac{(1+z_s)^2}{1+\alpha\gamma\mathscr{N}_{ss}^{-1}}}}{\sum_{s=-N}^{+N} \frac{1}{\left(1+\alpha\gamma\mathscr{N}_{ss}^{-1}\right)^{1/2}} e^{-\beta\gamma\frac{\ell^2}{d^2}\frac{(1+z_s)^2}{1+\alpha\gamma\mathscr{N}_{ss}^{-1}}}}. \tag{52}$$

The average value of the spin variable, from Eq.(21), assumes the form

$$\langle s \rangle = \frac{\sum_{s=-N}^{+N} \frac{s}{\left(1+\alpha\gamma\mathscr{N}_{ss}^{-1}\right)^{1/2}} e^{-\beta\gamma\frac{\ell^2}{d^2}\frac{(1+z_s)^2}{1+\alpha\gamma\mathscr{N}_{ss}^{-1}}}}{\sum_{s=-N}^{+N} \frac{1}{\left(1+\alpha\gamma\mathscr{N}_{ss}^{-1}\right)^{1/2}} e^{-\beta\gamma\frac{\ell^2}{d^2}\frac{(1+z_s)^2}{1+\alpha\gamma\mathscr{N}_{ss}^{-1}}}}. \tag{53}$$

The positions of the moving substrate wells, from Eq.(24), are given by

$$\frac{\langle \vec{y} \rangle}{d} = \frac{\ell}{d} \frac{\sum_{s=-N}^{+N} \frac{\alpha\gamma(1+z_s)\mathscr{N}^{-1}\vec{e}_s}{\left(1+\alpha\gamma\mathscr{N}_{ss}^{-1}\right)^{3/2}} e^{-\beta\gamma\frac{\ell^2}{d^2}\frac{(1+z_s)^2}{1+\alpha\gamma\mathscr{N}_{ss}^{-1}}}}{\sum_{s=-N}^{+N} \frac{1}{\left(1+\alpha\gamma\mathscr{N}_{ss}^{-1}\right)^{1/2}} e^{-\beta\gamma\frac{\ell^2}{d^2}\frac{(1+z_s)^2}{1+\alpha\gamma\mathscr{N}_{ss}^{-1}}}} - \frac{\ell}{d}\mathscr{N}^{-1}\vec{\eta}. \tag{54}$$

And finally, the probability density of the slider position is derived

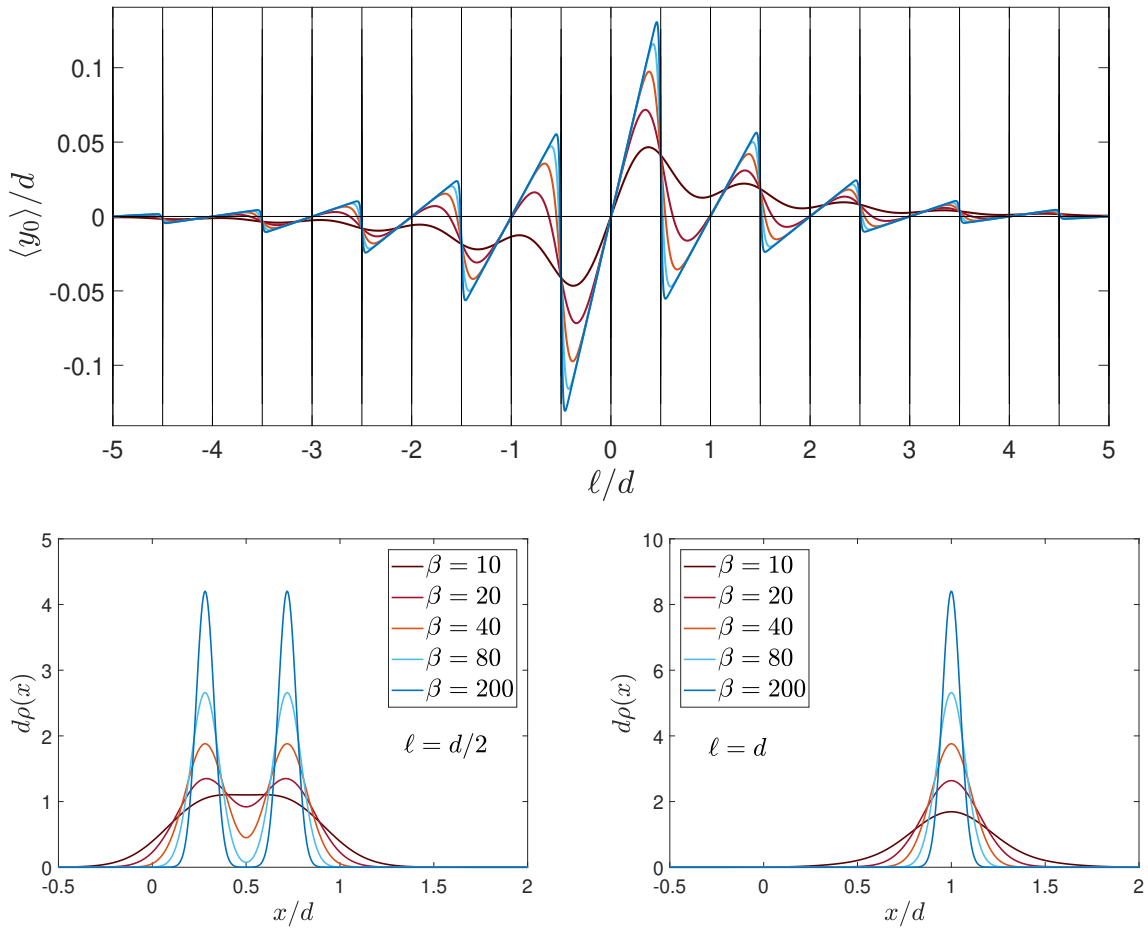

Fig. 3 Effect of the temperature on the substrate deformation and the probability density of x. We show the average substrate position $\langle y_0\rangle/d$ as function of ℓ/d for a chain with $N=5$ and for different values of β. Moreover, $d\rho(x)$ is plotted versus x/d for $\ell=d/2$ (bimodal distribution) and $\ell=d$ (monomodal distribution). We used the abscissa x/d and the ordinate $d\rho(x)$ in order to show a normalized curve with adimensional quantities. We adopted the parameters $k_L=4$, $k_S=3$, $k_W=8$, $k_D=5$, $d=1$, $K_BT=2/5,1/5,1/10,1/20,1/50$ in arbitrary units, corresponding to the following adimensional quantities: $\gamma=5/13$, $\lambda=3/4$, $\alpha=2$, $\beta=10,20,40,80,200$.

from Eq.(32) and is written as

$$\rho(x) = \frac{1}{d}\sqrt{\frac{\beta}{\pi(1-\gamma)}}e^{-\beta\frac{\gamma}{1-\gamma}\frac{\ell^2}{d^2}\left(1-\frac{x}{\ell}\right)^2} \times \frac{\sum_{s=-N}^{+N}\frac{1}{\left(1+\alpha\mathscr{N}_{ss}^{-1}\right)^{1/2}}e^{-\beta\frac{\ell^2}{d^2}\frac{\left(\frac{x}{\ell}+z_s\right)^2}{1+\alpha\mathscr{N}_{ss}^{-1}}}}{\sum_{s=-N}^{+N}\frac{1}{\left(1+\alpha\gamma\mathscr{N}_{ss}^{-1}\right)^{1/2}}e^{-\beta\gamma\frac{\ell^2}{d^2}\frac{(1+z_s)^2}{1+\alpha\gamma\mathscr{N}_{ss}^{-1}}}}. \quad (55)$$

As already mentioned, these formulas are particularly effective because they can be implemented by means of a single inverse matrix. This means that the sums appearing in these results are performed on terms that are immediately available and do not require any further computational cost.

Examples of applications of these results can be found in Figs.2-5. We consider a system with $N=5$, thus composed of $2N+1=11$ potential wells in the corrugated substrate, and we move the slider from $\ell/d=-N$ to $\ell/d=N$. We are interested in exploring the behavior of the system in terms of temperature and substrate stiffness. On the one hand, in Figs.2 and 3, we analyse the system with a varying temperature, i.e. with a parameter $\beta=k_Wd^2/(2K_BT)$ variable in the range from 10 to 200. On the other hand, in Figs.4 and 5, we analyse the system with a varying substrate stiffness, i.e. with a parameter $\lambda=k_S/k_L$ variable in the range from 0.083 to 7.5.

In Fig.2, one finds the average value of the spin variable $\langle s\rangle$, the average value of the normalized stick-slip force $\langle f\rangle/(k_wd)$, and the substrate positions vector $\langle\vec{y}\rangle/d$. The behavior of $\langle s\rangle$ simply shows that, as ℓ increases, the cursor hops from one energy well to the next. Due to thermal fluctuations, these transitions are sharper at low temperatures and smoother at high temperatures. Moreover, the plot of $\langle f\rangle/(k_wd)$ represents the stick-slip force versus the device position ℓ. We clearly see that the maximum of the force is increasing with β and therefore decreasing with the temperature T. This behavior explains the thermolubricity phenomenon as follows: the thermal fluctuations promote the crossing of energy barriers between wells and ultimately reduce static friction. Concerning $\langle\vec{y}\rangle/d$, we observe that the motion of

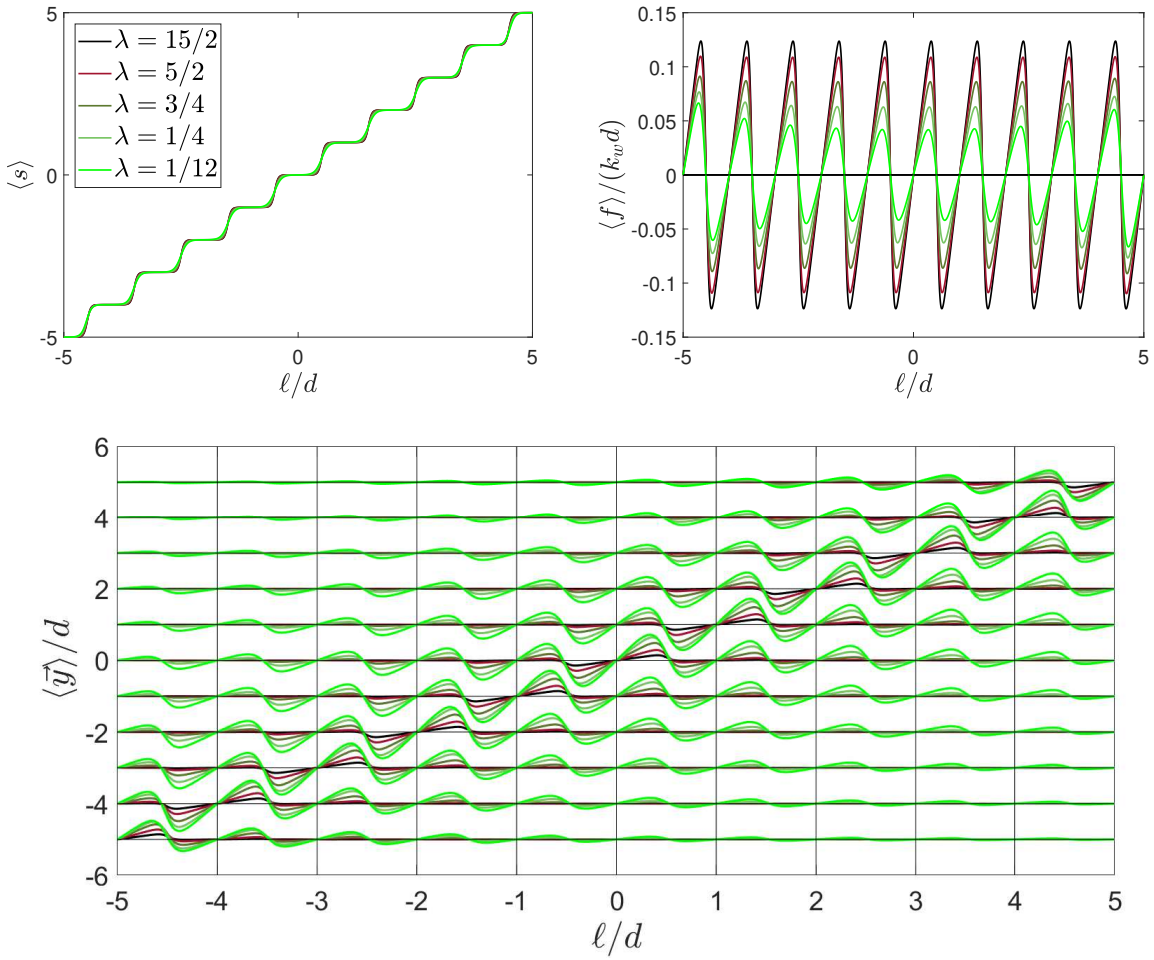

Fig. 4 Effect of the substrate stiffness on the stick-slip process. We show the average value of the spin variable $\langle s \rangle$, the average value of the normalized stick-slip force $\langle f \rangle/(k_w d)$, and the substrate positions vector $\langle \vec{y} \rangle/d$ as function of ℓ/d for a chain with $N = 5$ and for different values of λ. We adopted the parameters $k_L = 4$, $k_S = 1/3, 1, 3, 10, 30$, $k_W = 8$, $k_D = 5$, $d = 1$, $K_B T = 1/10$ in arbitrary units, corresponding to the following adimensional quantities: $\gamma = 5/13$, $\lambda = 1/12, 1/4, 3/4, 5/2, 15/2$, $\alpha = 2$, $\beta = 40$. In order to better visualize the behavior of the normalized positions $\langle y_j \rangle/d$, $-N \le j \le +N$, we plotted the curves $(\langle y_j \rangle/d - j)\mathscr{A} + j$, $-N \le j \le +N$, where we adopted the amplification factor $\mathscr{A} = 5$.

the slider affects the positions of the substrate wells and therefore generates a substrate deformation. The effect of this deformation is stronger for sites close to the moving cursor and negligible in distant areas. The extent of the deformed area depends on the longitudinal elastic constant k_L whereas the intensity of the deformation depends on the shear elastic constant k_S. Furthermore, this deformation is very small when the slider is in the center of the potential wells or on top of the barriers. Concerning the temperature effects, we observe that the substrate deformation is reduced with an increasing temperature since the thermal fluctuations facilitate the crossing of barriers reducing the interaction force between slider and substrate (coherently with the reduction of the static friction).

The average normalized position $\langle y_0 \rangle/d$ of the central energy well is plotted versus ℓ/d in Fig.3 in order to better discuss some details. We suppose to start the sliding process with the device at $\ell/d = 0$ and we move it rightwards. For $0 \le \ell/d < 1/2$, we observe a positive value for $\langle y_0 \rangle/d$, which is justified by the fact that to try to exit the central energy well we apply a positive force that tends to move the well itself to the right: this is at the origin of the deformation of the substrate. When we reach the potential barrier with the device at $\ell/d = 1/2$, we observe a rather complex phenomenon. The quantity $\langle y_0 \rangle/d$ is not zero as one might expect but takes on a positive value. A zero deformation should be expected as the maximum of the potential barrier is an unstable but stationary point with presumed zero interaction force between slider and substrate. Nevertheless, we must consider that the position ℓ of the device is deterministic but the position x of the slider is random and described by statistical mechanics as seen above. We know in fact its probability density given in Eq.(55), and represented in Fig.3 for $\ell = d/2$ (the first energy barrier on the right of the central well) and for $\ell = d$ (the center of the first energy well after the central one). It is important to observe that the instability corresponding to the energy barrier at $\ell = d/2$ generates a bimodal density for the variable x. It means that the slider is statistically split into two equivalent sliders, each residing in one of two adjacent wells centered at $x = 0$ and $x = d$. These two virtual sliders apply two opposite forces to the centers of the wells

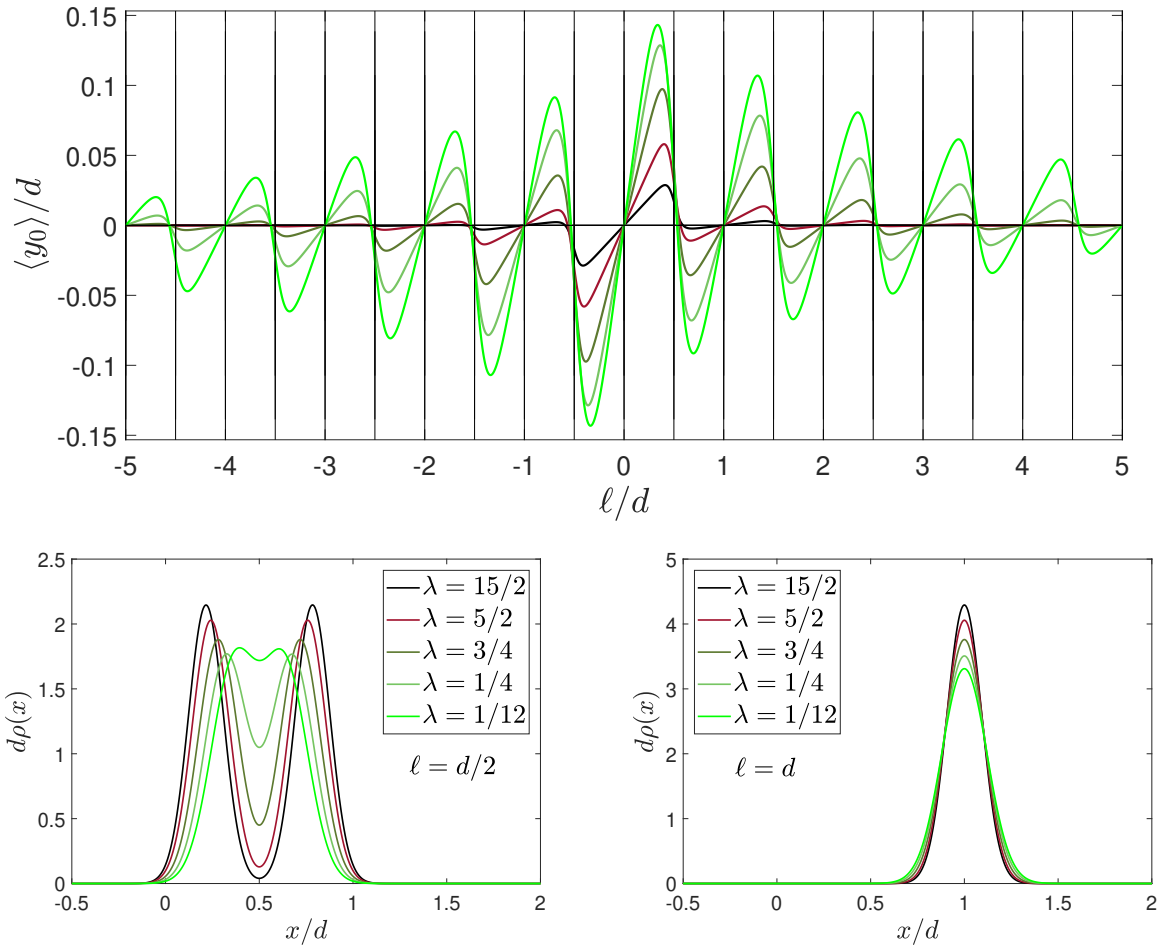

Fig. 5 Effect of the substrate stiffness on the substrate deformation and the probability density of x. We show the average substrate position $\langle y_0\rangle/d$ as function of ℓ/d for a chain with $N=5$ and for different values of λ. Moreover, $d\rho(x)$ is plotted versus x/d for $\ell=d/2$ (bimodal distribution) and $\ell=d$ (monomodal distribution). We used the abscissa x/d and the ordinate $d\rho(x)$ in order to show a normalized curve with adimensional quantities. We adopted the parameters $k_L=4$, $k_S=1/3,1,3,10,30$, $k_W=8$, $k_D=5$, $d=1$, $K_BT=1/10$ in arbitrary units, corresponding to the following adimensional quantities: $\gamma=5/13$, $\lambda=1/12,1/4,3/4,5/2,15/2$, $\alpha=2$, $\beta=40$.

centered at $x=0$ and $x=d$. Then, the bimodal distribution induces a decrease in the distance of the two centers and thus an increase of $\langle y_0\rangle/d$ and a decrease of $\langle y_1\rangle/d$, for $\ell=d/2$. This phenomenon is larger when the temperature is larger (see the case with $\beta=10$ in Fig.3) since the two virtual sliders are closer to the barrier for higher temperature. Therefore, they apply a larger force that brings the two wells closer together, sensibly increasing $\langle y_0\rangle/d$. The same process can be also observed for the successive energy barriers placed at $\ell=3d/2,5d/2,...$ and so on. Indeed, we see a positive value of $\langle y_0\rangle/d$ for these values of ℓ.

If we now look at the probability density of x for $\ell=d$, i.e. when the position of the traction device corresponds to the center of first potential well after the central one, we observe a monomodal distribution. However, for large temperatures, this density can be sensibly different from zero outside the region of the first potential well, representing a statistical dispersion of the slider over more than one potential well (in Fig.3, it is true for the case with $\beta=10$). It means that we can have $\langle y_0\rangle/d>0$ at $\ell/d=1,2,3,...$ for large values of the temperature. This particular effect, giving $\langle y_0\rangle/d>0$ for $\ell=d/2,3d/2,5d/2,...$ and $\ell=d,2d,3d,...$, has been carefully checked and confirmed also without taking into consideration the approximation introduced by the spin variable approach. In fact, a numerical approach to the problem provided the same results. For the sake of brevity we do not report here the details of this calculation.

In Fig.4, we can observe the effect of the substrate stiffness, quantified by $\lambda=k_S/k_L$, on the average value of the spin variable $\langle s\rangle$, on the average value of the normalized stick-slip force $\langle f\rangle/(k_w d)$, and on the substrate positions vector $\langle\vec{y}\rangle/d$. We considered here a fixed value for the temperature. We can see that the substrate stiffness slightly modifies the hopping among the potential wells described by $\langle s\rangle$. Instead, the stick-slip force and the substrate deformation are sensibly influenced by the substrate stiffness. We observe that with an increasing substrate stiffness, we have an increasing stick-slip force and a decreasing substrate deformation. We emphasize the fact that the behavior with a variable temperature was different. Indeed, as the temperature increased, both stick-slip force and substrate deformation were

found to decrease.

In Fig.5, we show the zoom of the normalized position $\langle y_0\rangle/d$ versus the slider position ℓ/d. As before, we can observe the oscillatory variation of $\langle y_0\rangle/d$ with a decrease of its intensity as the distance from the central point increases. Moreover, we see that $\langle y_0\rangle/d$ is slightly larger than zero for $\ell = d/2, 3d/2, 5d/2, ...$ and it is explained by the probability density of the variable x, which is bimodal in correspondance to the energy barriers, as one can find in Fig.5. In the plot of $\langle y_0\rangle/d$, we observe that for $\ell = d/2, 3d/2, 5d/2, ...$ the value of $\langle y_0\rangle/d$ increases with the decrease of λ. This exactly corresponds to the increasing distance between the two peaks in the probability density of x as the stiffness λ of the substrate increases. In fact if the two peaks are very close, they correspond to points with a high slope of the potential energy and apply a high force that produces a strong approaching of the energy wells. On the contrary, if the peaks are farther apart, they correspond to points having a lower slope of the potential energy and apply a lower force that tends to bring the energy wells closer to each other. Concerning the probability density of x for $\ell = d$, we observe that its value is nearly zero outside the energy well and therefore we see that $\langle y_0\rangle/d = 0$ for $\ell = d, 2d, 3d, ...$ This value can be increased only for larger values of the temperature.

Our model is based on equilibrium statistical mechanics and therefore we neglected frictional memory induced by finite speed, thermodynamic non-reversibility and substrate plasticity. For this reason, we cannot observe hysteresis in our frictional behaviour, an important feature present in several applications.[85,86] In addition, we completely neglected any nonlinear and/or nonlocal behaviour of the soft substrate in order to simplify the application of statistical mechanics. Some theoretical work in this direction can be found in the literature.[87,88]

4 The limit of the theory with an infinitely long substrate

We want to study here the behavior of the system with an infinitely long substrate ($N \to \infty$). To do this, we use some specific properties of tridiagonal matrices,[89,90] fully discussed in Appendix B. There, one can find an algorithm giving the closed form expressions for the elements of $\mathscr{N}^{-1}$. In particular, by means of this result, we can write the explicit expressions for the elements $\mathscr{N}^{-1}_{ss}$, representing the main diagonal of $\mathscr{N}^{-1}$. Indeed, by using Eqs.(106), (110) and (112) of Appendix B, we easily get $\mathscr{N}^{-1}_{ii} = \mathscr{G}(i)\mathscr{G}(M+1-i)/\mathscr{G}(M+1)$ with $1 \le i \le M$. By substituting $M = 2N+1$ and $i = s+N+1$ we obtain

$$\mathscr{N}^{-1}_{ss} = \frac{\mathscr{G}(s+N+1)\mathscr{G}(N+1-s)}{\mathscr{G}(2N+2)}, \tag{56}$$

where $-N \le s \le +N$. Here, the function $\mathscr{G}$ is defined as follows (see Eq.(111) in Appendix B)

$$\mathscr{G}(z) = \frac{1}{\sqrt{\Delta}}\left(\frac{2+\lambda+\sqrt{\Delta}}{2}\right)^z - \frac{1}{\sqrt{\Delta}}\left(\frac{2+\lambda-\sqrt{\Delta}}{2}\right)^z, \tag{57}$$

where $\Delta = \lambda^2+4\lambda$ (see Appendix B) and $\lambda = k_S/k_L$. We observe that in this function, the two fractions raised to the power z have the following properties: the first is larger than one, and the second is between zero and one. Since z is a function that grows linearly with N in the three $\mathscr{G}$ functions used in Eq.(56), if N is large, in Eq.(57) we can neglect the second power that tends to zero (the base is between zero and one) and we can keep only the first one (the base is larger than one). From Eq.(56), these premises deliver

$$\lim_{N\to\infty} \mathscr{N}^{-1}_{ss} = \frac{1}{\sqrt{\Delta}} = \frac{1}{\sqrt{\lambda^2+4\lambda}}, \tag{58}$$

showing that the diagonal of the inverse matrix of $\mathscr{N}$ is homogeneous in the limit of $N \to \infty$ ($\mathscr{N}^{-1}_{ss}$ does not depend on s). This is the first important result, which strongly simplifies the structures of previous results for large values of N. Second, we search for an explicit expression for z_s. By definition, it is given by $z_s = \vec{e}_s \cdot \mathscr{N}^{-1}\vec{\eta}$. Hence, since $(\vec{e}_s)_i = \delta_{s+N+1,i}$, we can write

$$\begin{aligned} z_s &= \sum_{j=1}^{2N+1} \mathscr{N}^{-1}_{s+N+1,j}\eta_j = \sum_{j=1}^{s+N} \mathscr{N}^{-1}_{s+N+1,j}\eta_j \\ &+ \mathscr{N}^{-1}_{s+N+1,s+N+1}\eta_{s+N+1} + \sum_{j=s+N+2}^{2N+1} \mathscr{N}^{-1}_{s+N+1,j}\eta_j, \end{aligned} \tag{59}$$

where the first sum is split into three parts, consistent with the expression of the inverse matrix given in Eq.(106) of the Appendix B. Therefore, in the first term we can substitute the values

$$\mathscr{N}^{-1}_{s+N+1,j} = \frac{\mathscr{G}(j)\mathscr{G}(N+1-s)}{\mathscr{G}(2N+2)}, \ (s+N+1 > j), \tag{60}$$

in the second one the following

$$\mathscr{N}^{-1}_{s+N+1,s+N+1} = \frac{\mathscr{G}(s+N+1)\mathscr{G}(N+1-s)}{\mathscr{G}(2N+2)}, \tag{61}$$

and in the third one

$$\mathscr{N}^{-1}_{s+N+1,j} = \frac{\mathscr{G}(s+N+1)\mathscr{G}(2N+2-j)}{\mathscr{G}(2N+2)}, \ (s+N+1 < j). \tag{62}$$

To sum up, we obtain the expression

$$\begin{aligned} z_s &= \sum_{j=1}^{s+N} \frac{\mathscr{G}(j)\mathscr{G}(N+1-s)}{\mathscr{G}(2N+2)}\eta_j \\ &+ \frac{\mathscr{G}(s+N+1)\mathscr{G}(N+1-s)}{\mathscr{G}(2N+2)}\eta_{s+N+1} \\ &+ \sum_{j=s+N+2}^{2N+1} \frac{\mathscr{G}(s+N+1)\mathscr{G}(2N+2-j)}{\mathscr{G}(2N+2)}\eta_j, \end{aligned} \tag{63}$$

where we must consider the components of the vector $\vec{\eta}$

$$\eta_j = (N+1)\frac{d}{\ell}\left(\delta_{j,1} - \delta_{j,N+1}\right) - (j-N-1)\frac{d}{\ell}\lambda. \tag{64}$$

Developing Eq.(63) with a long but straightforward calculation, we eventually obtain the following asymptotic behavior

$$\lim_{N\to\infty} z_s = -s\frac{d}{\ell}, \tag{65}$$

where $-\infty \leq s \leq +\infty$. It means that z_s depends linearly on s through the simple coefficient $-d/\ell$ when $N \to \infty$. The two results in Eqs.(58) and (65) are essential to obtain the explicit solutions describing the behaviour of the model with an infinitely long soft substrate.

We start from Eq.(53) giving the average value of the spin variable and we perform the limit for $N \to \infty$. By using Eqs. (58) and (65), we can rewrite Eq.(53) as follows

$$\langle s \rangle = \frac{\sum_{s=-\infty}^{+\infty} s e^{-\mu\left(\frac{\ell}{d}-s\right)^2}}{\sum_{s=-\infty}^{+\infty} e^{-\mu\left(\frac{\ell}{d}-s\right)^2}}, \tag{66}$$

where we introduced

$$\mu = \frac{\beta\gamma}{1+\alpha\gamma\frac{1}{\sqrt{\lambda^2+4\lambda}}} = \frac{\beta\gamma\sqrt{\lambda^2+4\lambda}}{\alpha\gamma+\sqrt{\lambda^2+4\lambda}} > 0. \tag{67}$$

The sum in the denominator can be easily written in the following closed form

$$\sum_{s=-\infty}^{+\infty} e^{-\mu\left(\frac{\ell}{d}-s\right)^2} = e^{-\mu\frac{\ell^2}{d^2}}\,\vartheta_3\left(-i\mu\frac{\ell}{d}, i\frac{\mu}{\pi}\right), \tag{68}$$

by using the third Jacobi theta function $\vartheta_3(z,\tau)$ defined below

$$\vartheta_3(z,\tau) = \sum_{n=-\infty}^{+\infty} e^{\pi i n^2\tau} e^{2inz} = 1 + 2\sum_{n=1}^{+\infty} e^{\pi i n^2\tau}\cos(2nz). \tag{69}$$

Here $z = -i\mu\ell/d \in \mathbb{C}$ is the argument, and $\tau = i\mu/\pi \in \mathbb{C}$ is the so-called lattice parameter satisfying the condition $\Im\mathrm{m}(\tau) > 0$.[91–95] Sometimes, also the nome $q = e^{i\pi\tau} = e^{-\mu}$ is introduced with the assumption $|q| < 1$, assuring the series convergence. This function satisfies the two relations

$$\vartheta_3(z+\pi,\tau) = \vartheta_3(z,\tau), \tag{70}$$

$$\vartheta_3(z+\pi\tau,\tau) = \frac{e^{-2iz}}{q}\,\vartheta_3(z,\tau), \tag{71}$$

stating that it is determined in the entire complex plane by the values it assumes in the parallelogram identified by the four points $z_0, z_0+\pi\tau, z_0+\pi+\pi\tau$ and $z_0+\pi\ \forall z_0 \in \mathbb{C}$ (the fundamental domain).[91–95] To write Eq.(68) in a more useful form, we can also introduce the following Jacobi functional identity for the third Jacobi theta function[94,95]

$$\vartheta_3(z,\tau) = \frac{1}{\sqrt{-i\tau}}\,e^{\frac{z^2}{\pi i\tau}}\,\vartheta_3\left(\frac{z}{\tau}, -\frac{1}{\tau}\right), \tag{72}$$

where the square root is to be interpreted as the principal value.[94,95] If we apply this identity to Eq.(68), we easily obtain

$$\sum_{s=-\infty}^{+\infty} e^{-\mu\left(\frac{\ell}{d}-s\right)^2} = \sqrt{\frac{\pi}{\mu}}\,\vartheta_3\left(-\pi\frac{\ell}{d}, i\frac{\pi}{\mu}\right). \tag{73}$$

Returning to Eq.(66), we note that the sum in the numerator can be written as function of the sum in the denominator as

$$\sum_{s=-\infty}^{+\infty} s e^{-\mu\left(\frac{\ell}{d}-s\right)^2} = \frac{d}{2\mu}\frac{\partial}{\partial\ell}\sum_{s=-\infty}^{+\infty} e^{-\mu\left(\frac{\ell}{d}-s\right)^2} + \frac{\ell}{d}\sum_{s=-\infty}^{+\infty} e^{-\mu\left(\frac{\ell}{d}-s\right)^2}, \tag{74}$$

and therefore we eventually obtain

$$\langle s \rangle = \frac{\ell}{d} - \frac{\pi}{2\mu}\frac{\vartheta_3'\left(-\pi\frac{\ell}{d}, i\frac{\pi}{\mu}\right)}{\vartheta_3\left(-\pi\frac{\ell}{d}, i\frac{\pi}{\mu}\right)}, \tag{75}$$

where $\vartheta_3' = \frac{\partial\vartheta_3}{\partial z}$. By using the following relation giving the logarithmic derivative of the third theta function[91–95]

$$\frac{\vartheta_3'(z,\tau)}{\vartheta_3(z,\tau)} = 4\sum_{n=1}^{+\infty}(-1)^n\frac{q^n}{1-q^{2n}}\sin(2nz), \tag{76}$$

which is valid for $|\Im\mathrm{m}(z)| < \frac{\pi}{2}\Im\mathrm{m}(\tau)$ and where $q = e^{i\pi\tau}$, we finally obtain

$$\langle s \rangle = \frac{\ell}{d} + \frac{2\pi}{\mu}\sum_{n=1}^{+\infty}(-1)^n\frac{e^{-\frac{n\pi^2}{\mu}}}{1-e^{-\frac{2n\pi^2}{\mu}}}\sin\left(2\pi n\frac{\ell}{d}\right). \tag{77}$$

This relationship is particularly clear from a physical point of view as the first term, linear in ℓ, represents the movement of the slider and the second term, described by a Fourier series, represents the periodicity of the infinite substrate. The resulting stepped curve is easily interpreted as a succession of jumps between the potential wells of the substrate. Interestingly enough, this process is controlled by only one parameter, namely μ defined in Eq.(67), taking into account the compromise between temperature (i.e. β), substrate elasticity (i.e. λ) and device elasticity (i.e. γ). In the case with $\lambda \to \infty$, we obtain an infinite rigid substrate. Under this condition, $\mu \to \beta\gamma$ and Eq.(77) becomes coincident with recent results obtained for undeformable substrates.[78] This comparison confers even more meaning to the expression of μ given in Eq.(67), which takes a modified form for finite values of substrate elasticity with respect to the value $\mu = \beta\gamma$, already known for rigid substrates.[78]

Concerning the stick-slip force on the soft substrate, by using Eqs. (58) and (65), we can rewrite Eq.(52) as follows

$$\frac{\langle f \rangle}{k_w d} = \frac{\gamma}{1+\alpha\gamma\frac{1}{\sqrt{\lambda^2+4\lambda}}}\frac{\sum_{s=-\infty}^{+\infty}\left(\frac{\ell}{d}-s\right)e^{-\mu\left(\frac{\ell}{d}-s\right)^2}}{\sum_{s=-\infty}^{+\infty} e^{-\mu\left(\frac{\ell}{d}-s\right)^2}}, \tag{78}$$

which can be simply written as

$$\begin{aligned}\frac{\langle f \rangle}{k_w d} &= \frac{\gamma}{1+\alpha\gamma\frac{1}{\sqrt{\lambda^2+4\lambda}}}\left(\frac{\ell}{d}-\langle s\rangle\right) = \frac{\pi}{2\beta}\frac{\vartheta_3'\left(-\pi\frac{\ell}{d}, i\frac{\pi}{\mu}\right)}{\vartheta_3\left(-\pi\frac{\ell}{d}, i\frac{\pi}{\mu}\right)} \\ &= \frac{2\pi}{\beta}\sum_{n=1}^{+\infty}(-1)^{n+1}\frac{e^{-\frac{n\pi^2}{\mu}}}{1-e^{-\frac{2n\pi^2}{\mu}}}\sin\left(2\pi n\frac{\ell}{d}\right),\end{aligned} \tag{79}$$

which is a Fourier series representing the periodic rate-independent stick-slip force on the infinitely long soft substrate. This result, too, has an explicit physical significance in that the

Fourier series makes it possible to evaluate the exact profile of the static friction force during the motion of the slider, and in particular its maximum value, which represents the threshold of force to be overcome in order to allow motion. The force shape during the slider motion is completely controlled by the two parameters β and μ. The important issue is that the force is highly dependent on the deformability of the substrate and on the system temperature. This can be easily seen for low values of the temperatures. Indeed, Eq.(79) allows a simple analysis for $T \to 0$. Indeed, by using the limit $\lim_{z\to 0} z/(1-e^{-az}) = 1/a$, Eq.(79) delivers

$$\lim_{T\to 0} \frac{\langle f \rangle}{k_w d} = \frac{1}{2\pi} \frac{\gamma\sqrt{\lambda^2+4\lambda}}{\alpha\gamma+\sqrt{\lambda^2+4\lambda}} \sum_{n=1}^{+\infty} (-1)^{n+1} \frac{2}{n} \sin\left(2\pi n \frac{\ell}{d}\right), \quad (80)$$

where we can recognize the Fourier series of a sawtooth wave

$$r = \sum_{n=1}^{+\infty} (-1)^{n+1} \frac{2}{n} \sin nr, \; r \in (-\pi, +\pi), \quad (81)$$

thus obtaining

$$\lim_{T\to 0} \frac{\langle f \rangle}{k_w d} = \frac{\gamma\sqrt{\lambda^2+4\lambda}}{\alpha\gamma+\sqrt{\lambda^2+4\lambda}} \frac{\ell}{d} = \frac{\frac{k_D}{k_W+k_D}\sqrt{\frac{k_S^2}{k_L^2}+4\frac{k_S}{k_L}}}{\frac{k_W}{k_L}\frac{k_D}{k_W+k_D}+\sqrt{\frac{k_S^2}{k_L^2}+4\frac{k_S}{k_L}}} \frac{\ell}{d}, \quad (82)$$

or

$$\lim_{T\to 0} \langle f \rangle = \frac{\frac{k_W k_D}{k_W+k_D}\sqrt{k_S^2+4k_S k_L}}{\frac{k_W k_D}{k_W+k_D}+\sqrt{k_S^2+4k_S k_L}} \ell = \frac{1}{\frac{1}{k_D}+\frac{1}{k_W}+\frac{1}{\sqrt{k_S^2+4k_S k_L}}} \ell, \quad (83)$$

for any ℓ such that $-1/2 < \ell/d < 1/2$, *i.e.* in the central energy well with undeformed position at $x = 0$. This result represents the purely mechanical force (without temperature effects) necessary to maintain the particle at position ℓ when it is pulled by the device with elastic constant k_D and attracted by the central well (elastic constant k_W) placed within the corrugated substrate with elastic properties k_S (shear) and k_L (longitudinal). From Eq.(83) we can deduce that the stick-slip force increases with an increasing device stiffness, with an increasing well stiffness, and with an increasing substrate stiffness. If the substrate is non-deformable (i.e. $k_S/k_L \to \infty$), we get

$$\lim_{k_S/k_L\to\infty} \lim_{T\to 0} \frac{\langle f \rangle}{k_w d} = \gamma \frac{\ell}{d} = \frac{k_D}{k_W+k_D} \frac{\ell}{d}, \quad (84)$$

which exactly corresponds to the purely mechanical force necessary to maintain the particle at position ℓ in the well with elastic constant k_0 and pulled by the spring with constant k. The theory is therefore perfectly consistent with the pure mechanics at $T = 0$. Moreover, if we consider a rigid substrate in Eq.(79), i.e. with $\lambda \to \infty$ or $\mu \to \beta\gamma$, we obtain the stick-slip force for a slider on an infinite undeformable substrate, as obtained in recent literature.[78]

We can now study the deformation of the infinite substrate induced by the slider motion. To do this, we use Eq.(54) and we can only focus on y_0 (coordinate of the central particle in Fig.1) since all components y_i have the same behaviour when the substrate is infinitely long. In order to develop Eq.(54) for y_0, we observe that the contribution of $\mathscr{N}^{-1}\vec{\eta}$ is zero (last term of Eq.(54)), and then we only need to evaluate $\mathscr{N}^{-1}\vec{e}_s$ (in the numerator of Eq.(54)). We note that the central component of $\mathscr{N}^{-1}\vec{e}_s$ is given by $\mathscr{N}^{-1}_{N+1,j}$ with $1 \le j \le 2N+1$. Hence, through Eq.(106), we calculate $\mathscr{N}^{-1}_{N+1,j}$ for large values of N as follows

$$\begin{aligned} \mathscr{N}^{-1}_{N+1,j} &= \frac{\mathscr{G}(j)\mathscr{G}(N+1)}{\mathscr{G}(2N+2)} \\ &\simeq \frac{1}{\sqrt{\Delta}} \left(\frac{2+\lambda+\sqrt{\Delta}}{2}\right)^{N+1-j}, \forall j \le N+1, \quad (85) \\ \mathscr{N}^{-1}_{N+1,j} &= \frac{\mathscr{G}(N+1)\mathscr{G}(2N+2-j)}{\mathscr{G}(2N+2)} \\ &\simeq \frac{1}{\sqrt{\Delta}} \left(\frac{2+\lambda+\sqrt{\Delta}}{2}\right)^{j-N-1}, \forall j > N+1, \quad (86) \end{aligned}$$

or, equivalently,

$$\lim_{N\to\infty} \mathscr{N}^{-1}_{N+1,j} = \frac{1}{\sqrt{\Delta}} \left(\frac{2+\lambda+\sqrt{\Delta}}{2}\right)^{-|j-N-1|}, \forall 1 \le j \le 2N+1. \quad (87)$$

Therefore, we have that $\mathscr{N}^{-1}\vec{e}_s$ simply provides a contribution equal to $\frac{1}{\sqrt{\Delta}}[(2+\lambda+\sqrt{\Delta})/2]^{-|s|}$ for the position y_0 in Eq.(54) (here $-N \le s \le +N$). Then, we obtain

$$\frac{\langle y_0 \rangle}{d} = \frac{\alpha\gamma}{\alpha\gamma+\sqrt{\Delta}} \frac{\sum_{s=-\infty}^{+\infty} \left(\frac{\ell}{d}-s\right) \left(\frac{2+\lambda+\sqrt{\Delta}}{2}\right)^{-|s|} e^{-\mu\left(\frac{\ell}{d}-s\right)^2}}{\sum_{s=-\infty}^{+\infty} e^{-\mu\left(\frac{\ell}{d}-s\right)^2}}. \quad (88)$$

While the sum in the denominator has been already calculated in Eq.(68) or in Eq.(73), to evaluate the sum in the numerator we need to introduce the so-called partial theta function

$$\vartheta_3^P(z,\tau) = \sum_{n=0}^{+\infty} e^{\pi i n^2 \tau} e^{2inz}, \quad (89)$$

where the exponent P means *partial*. As there are many rather heterogeneous notations for this function,[96–98] we prefer to define it as the complete theta function given in Eq.(69) but summing only over values of n greater than or equal to zero ($n \ge 0$). A long but straightforward elaboration of Eq.(88) leads to the explicit result

$$\frac{\langle y_0 \rangle}{d} = \frac{\alpha\gamma}{\alpha\gamma+\sqrt{\lambda^2+4\lambda}} \frac{\mathscr{M}}{\vartheta_3\left(-i\mu\frac{\ell}{d}, i\frac{\mu}{\pi}\right)}, \quad (90)$$

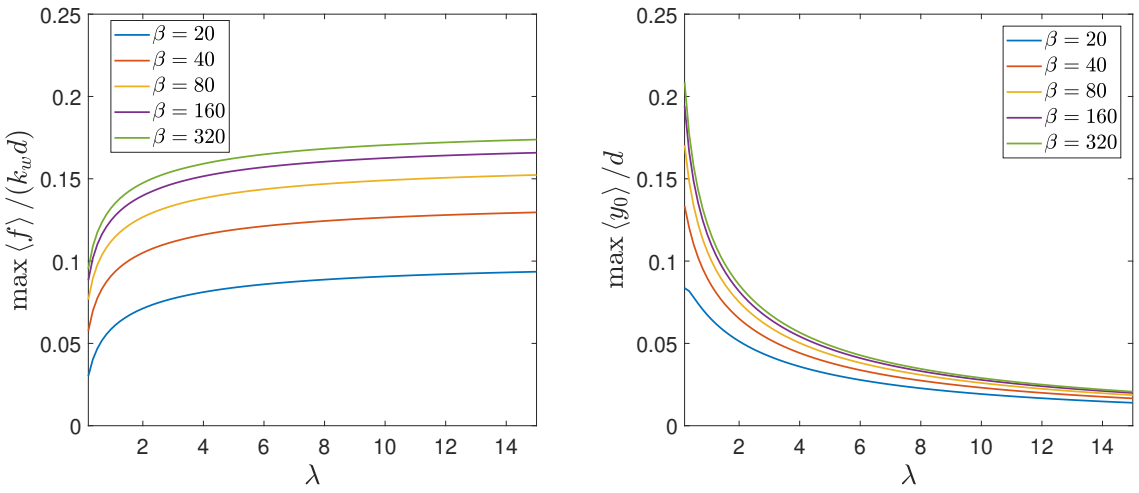

Fig. 6 Effect of the substrate stiffness on the stick-slip force, represented by $\max\langle f\rangle/(k_W d)$, and on the substrate deformation, represented by $\max\langle y_0\rangle/d$. We considered an infinitely long substrate described by Eqs.(77), (79), (90), and (94). We adopted the parameters $k_L=4$, $k_S\in(0.8,60)$, $k_W=8$, $k_D=5$, $d=1$, $K_BT=1/5,1/10,1/20,1/40,1/80$ in arbitrary units, corresponding to the following adimensional quantities: $\gamma=5/13$, $\alpha=2$, $\beta=20,40,80,160,320$, $\lambda\in(0.2,15)$.

where

$$\begin{aligned}\mathscr{M} &= \frac{\ell}{d}\vartheta_3^P\left[i\left(\log\sqrt{\frac{2+\lambda+\sqrt{\Delta}}{2}}-\mu\frac{\ell}{d}\right),i\frac{\mu}{\pi}\right] \\ &+\frac{\ell}{d}\vartheta_3^P\left[i\left(\log\sqrt{\frac{2+\lambda+\sqrt{\Delta}}{2}}+\mu\frac{\ell}{d}\right),i\frac{\mu}{\pi}\right] \\ &-\frac{1}{2i}\left(\vartheta_3^P\right)'\left[i\left(\log\sqrt{\frac{2+\lambda+\sqrt{\Delta}}{2}}-\mu\frac{\ell}{d}\right),i\frac{\mu}{\pi}\right] \\ &+\frac{1}{2i}\left(\vartheta_3^P\right)'\left[i\left(\log\sqrt{\frac{2+\lambda+\sqrt{\Delta}}{2}}+\mu\frac{\ell}{d}\right),i\frac{\mu}{\pi}\right]-\frac{\ell}{d},\end{aligned} \tag{91}$$

with $\left(\vartheta_3^P\right)'(z,\tau)=\frac{\partial}{\partial z}\vartheta_3^P(z,\tau)$. Unfortunately, no particular properties of the partial theta function are available to further simplify the structure of this result.

To conclude, we can evaluate the probability density $\rho(x)$ for a system with an infinitely long substrate. We use Eq.(55) where we apply Eqs. (58) and (65) and we obtain

$$\begin{aligned}\rho(x) &= \frac{1}{d}\sqrt{\frac{\beta}{\pi(1-\gamma)}}e^{-\beta\frac{\gamma}{1-\gamma}\left(\frac{\ell}{d}-\frac{x}{d}\right)^2} \\ &\times\sqrt{\frac{\alpha\gamma+\sqrt{\lambda^2+4\lambda}}{\alpha+\sqrt{\lambda^2+4\lambda}}}\frac{\sum_{s=-\infty}^{+\infty}e^{-\nu\left(\frac{x}{d}-s\right)^2}}{\sum_{s=-\infty}^{+\infty}e^{-\mu\left(\frac{\ell}{d}-s\right)^2}},\end{aligned} \tag{92}$$

where ν is defined as follows

$$\nu=\frac{\beta}{1+\alpha\frac{1}{\sqrt{\lambda^2+4\lambda}}}=\frac{\beta\sqrt{\lambda^2+4\lambda}}{\alpha+\sqrt{\lambda^2+4\lambda}}>0, \tag{93}$$

in a similar way to what we did with μ in Eq.(67). Now, we can use the sum calculated in Eq.(73), finally obtaining the probability density

$$\rho(x)=\frac{1}{d}\sqrt{\frac{\gamma\beta}{\pi(1-\gamma)}}e^{-\beta\frac{\gamma}{1-\gamma}\left(\frac{\ell}{d}-\frac{x}{d}\right)^2}\frac{\vartheta_3\left(-\pi\frac{x}{d},i\frac{\pi}{\nu}\right)}{\vartheta_3\left(-\pi\frac{\ell}{d},i\frac{\pi}{\mu}\right)}. \tag{94}$$

Interestingly enough, we can check the normalization condition stated in Eq.(26). To do this, it is possible to prove by a direct calculation the following property

$$\begin{aligned}&\int_{-\infty}^{+\infty}e^{-\varepsilon\left(\frac{\ell}{d}-\frac{x}{d}\right)^2}\vartheta_3\left(-\pi\frac{x}{d},i\frac{\pi}{\nu}\right)\mathrm{d}x \\ &=d\sqrt{\frac{\pi}{g}}\vartheta_3\left[-\pi\frac{\ell}{d},i\pi\left(\frac{1}{\nu}+\frac{1}{\varepsilon}\right)\right],\end{aligned} \tag{95}$$

which is valid for any value of ε. If we suppose that $\varepsilon=\gamma\beta/(1-\gamma)$, we simply have that $1/\nu+1/\varepsilon=1/\mu$ (it is sufficient to use Eqs.(67) and (93)), and then Eq.(95) immediately proves the normalization condition for Eq.(94), stated in Eq.(26).

To conclude, the infinitely long substrate is described by the solutions given in Eqs.(77), (79), (90), and (94), representing the average spin variable, the average stick-slip force, the average substrate deformation, and the probability density of the x variable, respectively. These results, in addition to being particularly elegant in that they disclose a connection between the stick-slip problem with the third Jacobi theta function $\vartheta_3(z,\tau)$ theory, are useful for obtaining a summary of the behavior of the system composed of slider and soft substrate. In Fig.6, we show the infinite system behavior with a varying substrate stiffness, and in Fig.7 its behavior with a varying device stiffness. It can be seen from Fig.6 that while the average static friction force increases with increasing substrate stiffness, the deformation of the substrate itself decreases with its stiffness. This corresponds with what is ob-

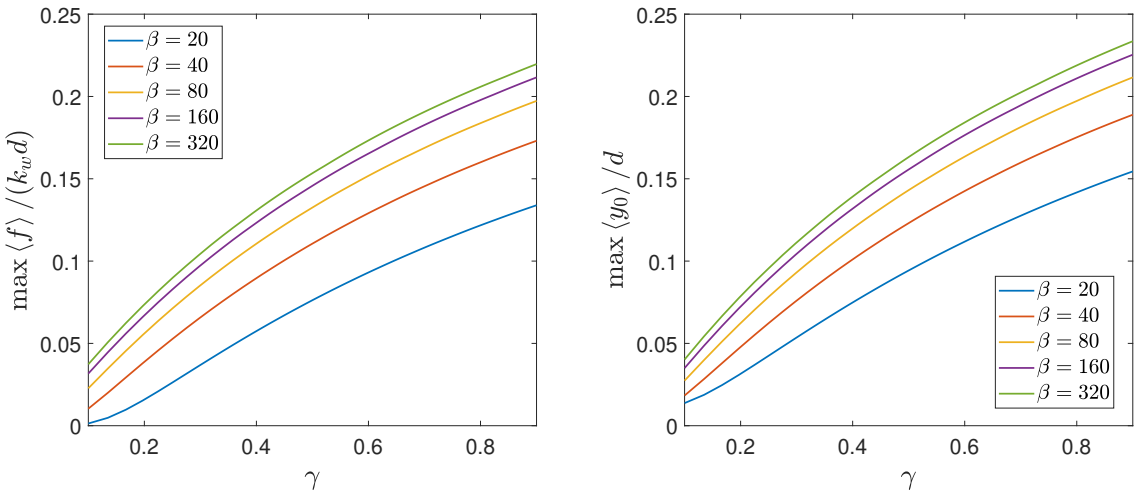

Fig. 7 Effect of the device stiffness on the stick-slip force, represented by $\max \langle f \rangle / (k_W d)$, and on the substrate deformation, represented by $\max \langle y_0 \rangle / d$. We considered an infinitely long substrate described by Eqs.(77), (79), (90), and (94). We adopted the parameters $k_L = 4$, $k_S = 3$, $k_W = 8$, $k_D \in (8/9, 72)$, $d = 1$, $K_B T = 1/5, 1/10, 1/20, 1/40, 1/80$ in arbitrary units, corresponding to the following adimensional quantities: $\gamma \in (0.1, 0.9)$, $\alpha = 2$, $\beta = 20, 40, 80, 160, 320$, $\lambda = 3/4$.

served in Fig.4, and this is also in good agreement with the recent results obtained for the stochastic sliding friction (for low velocities of the slider).[47] Moreover, we also see that the average static friction force and the deformation of the substrate decrease as temperature increases, as already observed in Fig.2. Similarly, we see in Fig.7 the effect of the device stiffness. We directly deduce that both the average static friction force and the deformation of the substrate increase with the parameter γ and decrease with the temperature.

We observed that the temperature is always able to reduce the stick-slip force or, equivalently, the static friction. This behaviour falls into the class of superlubricity phenomena, and is tipically referred to as thermolubricity.[99,100] Of course, the decrease of friction with temperature is also predicted in the original Prandtl-Tomlinson model with rigid substrate since thermal energy fosters the crossing of energy barriers.[23–33] Interestingly, this behavior has been confirmed by experiments conducted on various materials using the atomic force microscope.[101,102]

To conclude the discussion concerning the infinitely long substrate, we show in Fig.8 some plots of the probability density of the variable x. More specifically, one can see the surface representing $d\rho(x)$ in terms of the variable x/d and of the parameter ℓ/d. Of course, the curve of $d\rho(x)$ versus x/d is normalized (the underlying area is unitary) for any value of ℓ/d, as stated in Eq.(26). We considered different values of the temperature and of the substrate stiffness, in order to better show the system behavior. First of all, we remark that the character of the curve $d\rho(x)$ versus x/d is monomodal for $\ell/d = 0$ or $\ell/d = 1$, where the slider is in a stable configuration placed at the center of the quadratic wells of the corrugated substrate. Differently, the curve $d\rho(x)$ versus x/d is bimodal for $\ell/d = 1/2$, when the slider is in the unstable position at the top of the energy barrier between two adjacent potential wells. Hence, the three-dimensional plots in Fig.8 explain two peculiar behaviors of the system. Firstly, the bimodal character of the density for $\ell/d = 1/2$ induces a positive value of the substrate deformation, i.e. $\langle y_0 \rangle > 0$ for $\ell/d = 1/2$. Indeed, the slider is statistically equivalent to a couple of virtual sliders placed at the sides of the barrier and therefore these ones try to bring the two potential wells closer together ($\langle y_0 \rangle > 0$ and $\langle y_1 \rangle < 0$). Secondly, the monomodal character of the density, say for $\ell/d = 1$, explains the positive value of $\langle y_0 \rangle$ for $\ell/d = 1$ and for large values of the temperature. Indeed, if the temperature is sufficiently high, the tails of the probability density are non-negligible in the side wells centered in $x/d = 0$ and $x/d = 2$. These tails correspond to two virtual sliders that try to compress the central well, inducing $\langle y_0 \rangle > 0$ and $\langle y_2 \rangle < 0$. Of course, these phenomena are controlled by temperature and substrate stiffness, as one can appreciate from Fig.8.

We finally remark that the solutions given in Eqs.(77), (79), (90), and (94) fully describe the behavior of an infinitely long soft substrate and they represent the direct generalization of the results recently obtained for a rigid substrate,[78] performed by simlply substituting the product $\beta\gamma$ with the parameter μ defined in Eq.(67).

5 Conclusions

In this work we elaborated a modified Prandtl-Tomlinson model for describing the stick-slip phenomenon on a soft or deformable substrate. Instead of considering a sinusoidal corrugated substrate as in the original model, we introduced here a sequence of quadratic energy wells, which represent a more appropriate structure for the analytical development of the model. Importantly, we introduced the substrate elasticity by means of a spring ladder network, enabling the displacement of the substrate energy wells. On the one hand, the quadratic wells allow us to consider this structure to mimic the elasticity of the substrate, and on the other hand, they allow us to use the spin variable technique that enables us to work with complex, nonconcave potential energy. Indeed, we analyzed the quasi-static behavior of the stick-slip by

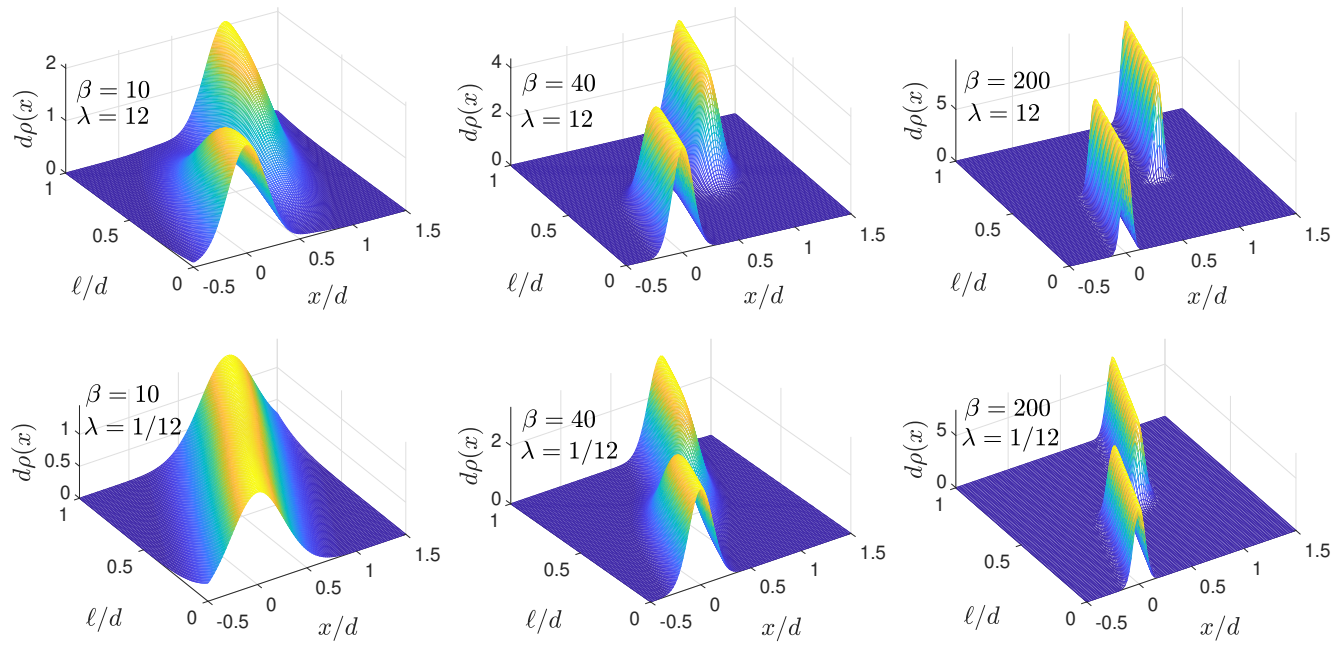

Fig. 8 Evolution of the probability density of the variable x with different values of the temperature and of the substrate stiffness. We used the abscissae x/d and ℓ/d and the ordinate $d\rho(x)$ in order to show a normalized curve on the plane $(x/d,d\rho)$, with adimensional quantities. We adopted the parameters $k_L = 4$, $k_S = 1/3,48$, $k_W = 8$, $k_D = 5$, $d = 1$, $K_BT = 2/5,1/10,1/50$ in arbitrary units, corresponding to the following adimensional quantities: $\gamma = 5/13$, $\alpha = 2$, $\beta = 10,40,200$, $\lambda = 1/12,12$.

means of the equilibrium statistical mechanics. It means that we suppose the system in contact with a thermal bath at a given temperature and we coherently use the canonical distribution of the statistical mechanics. As discussed, its partition function can be evaluated in closed for for our system. Hence, the model permits the determination of the static friction and the deformation of the substrate in terms of the thermal fluctuations and of the substrate stiffness. Moreover, we also analyze the average value of the spin variable representing the energy well explored during the slider motion, and the probability density of the slider position, which is useful to better understand the system behavior. Firstly, we proved that the stick-slip force (or quasi-static friction force) increases with the substrate stiffness and decreases with the temperature. Secondly, we provided evidence that the deformation of the substrate decreases with both substrate stiffness and temperature. These results briefly summarize the behavior of the stick-slip on a soft substrate. However, we show that refined phenomena can be noticed when the slider passes to the unstable position corresponding to the top of the barrier or to the stable position in the middle of the wells. Indeed, especially for nanoscopic systems, one must consider the probability density of the slider position, which can be nonnegligible in a spatial region of the same order as the extent of each energy well. Thus, this leads to observable effects on substrate deformation, which can be different from zero both with the slider at the tops of the barriers and with the slider in the potential minima. This again explains the complexity of the stick-slip phenomenon at the nanoscale where the effects of thermal fluctuations can be crucial.

While being a paradigmatic model for the description of the stick-slip process on a soft substrate, our structure should be improved to better represent more realistic situations. One drawback concerns the particular shape of the corrugated substrate. Although the sequence of parabolas is qualitatively similar to the Prandtl-Tomlinson model, other geometries can be imagined to achieve greater similarity with the original sinusoidal profile. For example, one could consider two or more energy levels for the intercalated wells. Another improvement concerns the dynamics of the frictional processes, which should be studied in the context of the out-of-equilibrium statistical mechanics.[103,104] There is in fact a complex interplay between the traction speed applied to the slider, the characteristic times induced by the stiffness of each well of the potential energy, and the times induced by the transition rates between the adjacent wells, which depend on the energy barrier as classically described by the Kramers theory.[105,106] In order to introduce non-equilibrium thermodynamics and irreversibility we can add to the conservative potential energy two terms (as done by Langevin for a single particle in a thermal bath): a dissipative term which can be considered as a viscous force (opposite and proportional to the velocity) and a noise term (with white gaussian behaviour for simplicity). This scheme converges to the equilibrium solution for long time but is able to reproduce all the out-of-equilibrium thermodynamics in an arbitrary time regime.[107,108]

To conclude, we can affirm that our proposed method to take into account the temperature effect and the soft substrate in stick-slip and frictional phenomena can be adopted for several problems, including the study of the cells motion and the development of new haptic and tactile technologies.

Appendix A: The inverse and the determinant of the matrix $\mathscr{B}+x\vec{b}\otimes\vec{b}$

We consider a matrix $\mathscr{B}\in\mathscr{M}_{M,M}(\mathbb{R})$ and a vector $\vec{b}\in\mathbb{R}^M$ such that $\mathscr{B}^{-1}$ and $\left(\mathscr{B}+x\vec{b}\otimes\vec{b}\right)^{-1}$ exist for some $x\in\mathbb{R}$. First of all, we prove Eq.(33) of the main text. To do this, we develop the matrix product

$$\begin{aligned}&\left(\mathscr{B}+x\vec{b}\otimes\vec{b}\right)\left(\mathscr{B}^{-1}-x\frac{\mathscr{B}^{-1}\vec{b}\otimes\vec{b}\mathscr{B}^{-1}}{1+x\vec{b}\cdot\mathscr{B}^{-1}\vec{b}}\right)\\ =\;&\mathscr{I}-x\frac{\vec{b}\otimes\vec{b}\mathscr{B}^{-1}}{1+x\vec{b}\cdot\mathscr{B}^{-1}\vec{b}}+x\vec{b}\otimes\vec{b}\mathscr{B}^{-1}-x^2\frac{\vec{b}\otimes\vec{b}\mathscr{B}^{-1}\vec{b}\otimes\vec{b}\mathscr{B}^{-1}}{1+x\vec{b}\cdot\mathscr{B}^{-1}\vec{b}}\\ =\;&\mathscr{I}-x\frac{\vec{b}\otimes\vec{b}\mathscr{B}^{-1}}{1+xy}+x\vec{b}\otimes\vec{b}\mathscr{B}^{-1}-x^2y\frac{\vec{b}\otimes\vec{b}\mathscr{B}^{-1}}{1+xy},\end{aligned}\tag{96}$$

where $y=\vec{b}\cdot\mathscr{B}^{-1}\vec{b}$. By simplifying the last sum, we obtain the result coinciding with the identical matrix $\mathscr{I}$, finally proving the first property stated in Eq.(33). Concerning the second property, we use the following theorem

$$\frac{d}{dx}\det\mathscr{A}=\det\mathscr{A}\,\mathrm{tr}\left(\mathscr{A}^{-1}\frac{d\mathscr{A}}{dx}\right),\tag{97}$$

which is valid for any non-singular x-dependent matrix $\mathscr{A}\in\mathscr{M}_{M,M}(\mathbb{R})$. We suppose now that $\mathscr{A}=\mathscr{B}+x\vec{b}\otimes\vec{b}$ and we obtain

$$\frac{d}{dx}\log\left[\det\left(\mathscr{B}+x\vec{b}\otimes\vec{b}\right)\right]=\mathrm{tr}\left[\left(\mathscr{B}+x\vec{b}\otimes\vec{b}\right)^{-1}\vec{b}\otimes\vec{b}\right].\tag{98}$$

From the first property just demonstrated we easily obtain

$$\frac{d}{dx}\log\left[\det\left(\mathscr{B}+x\vec{b}\otimes\vec{b}\right)\right]=\frac{y}{1+xy},\tag{99}$$

where $y=\vec{b}\cdot\mathscr{B}^{-1}\vec{b}$, as before. By integrating this relation over x, we get

$$\log\left[\det\left(\mathscr{B}+x\vec{b}\otimes\vec{b}\right)\right]-\log\left[\det\left(\mathscr{B}\right)\right]=\log(1+xy).\tag{100}$$

To conclude, applying the exponential function we prove the relation

$$\det\left(\mathscr{B}+x\vec{b}\otimes\vec{b}\right)=\det\mathscr{B}\left(1+x\vec{b}\cdot\mathscr{B}^{-1}\vec{b}\right),\tag{101}$$

corresponding to Eq.(34) of the main text.

Appendix B: Properties of the matrix $\mathscr{N}$

We prove here some properties concerning the tridiagonal matrices. To begin, we consider the following arbitrary tridiagonal matrix $\mathscr{T}$

$$\mathscr{T}=\begin{bmatrix}a_1&b_1&0&\cdots&0\\c_1&a_2&b_2&\ddots&\vdots\\0&c_2&\ddots&\ddots&0\\\vdots&\ddots&\ddots&a_{M-1}&b_{M-1}\\0&\cdots&0&c_{M-1}&a_M\end{bmatrix}\in\mathscr{M}_{M,M}(\mathbb{R}),\tag{102}$$

where the diagonal is composed by the elements $(a_1,...,a_M)$, the superdiagonal by $(b_1,...,b_{M-1})$ and the subdiagonal by $(c_1,...,c_{M-1})$. It has been proved[89,90] that the elements of the inverse matrix $\mathscr{T}^{-1}$ can be represented as

$$\left[\mathscr{T}^{-1}\right]_{ij}=\begin{cases}\frac{1}{\vartheta_M}(-1)^{i+j}b_i\times...\times b_{j-1}\vartheta_{i-1}\varphi_{j+1}, & i<j\\ \frac{1}{\vartheta_M}\vartheta_{i-1}\varphi_{i+1}, & i=j\\ \frac{1}{\vartheta_M}(-1)^{i+j}c_j\times...\times c_{i-1}\vartheta_{j-1}\varphi_{i+1}, & i>j\end{cases}\tag{103}$$

where the sequences ϑ_i and φ_i are given by the recursive laws

$$\begin{cases}\vartheta_i=a_i\vartheta_{i-1}-b_{i-1}c_{i-1}\vartheta_{i-2},\ \forall i=1,...,M,\\ \vartheta_{-1}=0,\vartheta_0=1,(\vartheta_1=a_1),\end{cases}\tag{104}$$

and

$$\begin{cases}\varphi_i=a_i\varphi_{i+1}-b_ic_i\varphi_{i+2},\ \forall i=M,...,1,\\ \varphi_{M+2}=0,\varphi_{M+1}=1,(\varphi_M=a_M).\end{cases}\tag{105}$$

While Eq.(104) is an increasing recursive law going from $i=1$ to $i=M$, Eq.(105) is a decreasing recursive law going from $i=M$ to $i=1$. We also remember that $\det\mathscr{T}=\vartheta_M$[89,90]. In the case of the matrix $\mathscr{N}$, we have that $b_i=-1\forall i$, $c_i=-1\forall i$, and $a_i=2+\lambda\forall i$. Under this hypothesis, the general result can be simplified as follows

$$\left[\mathscr{T}^{-1}\right]_{ij}=\begin{cases}\frac{1}{\vartheta_M}\vartheta_{i-1}\varphi_{j+1}, & i<j\\ \frac{1}{\vartheta_M}\vartheta_{i-1}\varphi_{i+1}, & i=j\\ \frac{1}{\vartheta_M}\vartheta_{j-1}\varphi_{i+1}, & i>j\end{cases}\tag{106}$$

where the sequences ϑ_i and φ_i are given by the reduced recursive laws

$$\begin{cases}\vartheta_i=(2+\lambda)\vartheta_{i-1}-\vartheta_{i-2},\ \forall i=1,...,M\\ \vartheta_{-1}=0,\vartheta_0=1,\end{cases}\tag{107}$$

and

$$\begin{cases}\varphi_i=(2+\lambda)\varphi_{i+1}-\varphi_{i+2},\ \forall i=M,...,1\\ \varphi_{M+2}=0,\varphi_{M+1}=1.\end{cases}\tag{108}$$

To begin, we consider Eq.(107) whose general solution can be written as

$$\vartheta_i=p\left(\frac{2+\lambda+\sqrt{\Delta}}{2}\right)^i+q\left(\frac{2+\lambda-\sqrt{\Delta}}{2}\right)^i,\tag{109}$$

with $\Delta=\lambda^2+4\lambda$ and where the coefficients p and q must be fixed through the conditions $\vartheta_{-1}=0$ and $\vartheta_0=1$. A straightforward calculation leads to the explicit solution

$$\vartheta_i=\mathscr{G}(i+1),\tag{110}$$

where the function $\mathscr{G}(z)$ is defined as follows

$$\mathscr{G}(z) = \frac{1}{\sqrt{\Delta}} \left(\frac{2+\lambda+\sqrt{\Delta}}{2} \right)^z - \frac{1}{\sqrt{\Delta}} \left(\frac{2+\lambda-\sqrt{\Delta}}{2} \right)^z. \quad (111)$$

A similar calculation leads to the solution of Eq.(108) in the form

$$\varphi_i = \mathscr{G}(M+2-i). \quad (112)$$

Finally, Eqs.(110) and (112) allow for the calculation of the inverse matrix when combined with Eq.(106).

Conflicts of interest

There are no conflicts to declare.

Notes and references

1 J. Gao, W. D. Luedtke, D. Gourdon, M. Ruths, J. N. Israelachvili, and Uzi Landman, Frictional Forces and Amontons' Law: From the Molecular to the Macroscopic Scale, *J. Phys. Chem. B*, 2004, **108**, 3410-3425.

2 M. Urbakh, J. Klafter, D. Gourdon, and J. Israelachvili, The nonlinear nature of friction, *Nature*, 2004, **430**, 525-528.

3 A. Vanossi, N. Manini, M. Urbakh, S. Zapperi, and E. Tosatti, Colloquium: Modeling friction: From nanoscale to mesoscale, *Rev. Mod. Phys.*, 2013, **85**, 529-552.

4 A.I. Vakis, V.A. Yastrebov, J. Scheibert, L. Nicola, D. Dini, C. Minfray, A. Almqvist, M. Paggi, S. Lee, G. Limbert, J. F. Molinari, G. Anciaux, R. Aghababaei, S. Echeverri Restrepo, A. Papangelo, A. Cammarata, P. Nicolini, C. Putignano, G. Carbone, S. Stupkiewicz, J. Lengiewicz, G. Costagliola, F. Bosia, R. Guarino, N.M. Pugno, M. H. Müser, M. Ciavarella, Modeling and simulation in tribology across scales: An overview, *Tribology International*, 2018, **125**, 169-199.

5 T. W. J. de Geus, M. Popovic, W. Ji, A. Rosso, and M. Wyart, How collective asperity detachments nucleate slip at frictional interfaces, *PNAS*, 2019, **116**, 23977-23983.

6 M. Ternes, C. P. Lutz, C. F. Hirjibehedin, F. J. Giessibl, and A. J. Heinrich, The Force Needed to Move an Atom on a Surface, *Science*, 2008, **319**, 1066-1069.

7 S. Y. Krylov, and J. W. M. Frenken, The physics of atomic-scale friction: Basic considerations and open questions, *Phys. Status Solidi*, 2014, **251**, 711-736.

8 N. Manini, G. Mistura, G. Paolicelli, E. Tosatti, and A. Vanossi, Current trends in the physics of nanoscale friction, *Advances in Physics: X*, 2017, **2**, 569-590.

9 E. Liamas, S. D. Connell, S. N. Ramakrishna, and A. Sarkar, Probing the frictional properties of soft materials at the nanoscale, *Nanoscale*, 2020, **12**, 2292.

10 V. Bormuth, V. Varga, J. Howard, and E. Schäffer, Protein Friction Limits Diffusive and Directed Movements of Kinesin Motors on Microtubules, *Science*, 2009, **325**, 870.

11 P. Sens, Stick–slip model for actin-driven cell protrusions, cell polarization, and crawling, *PNAS*, 2020, **117**, 24670-24678.

12 G. A. Ateshian, and H. Wang, A theoretical solution for the frictionless rolling contact of cylindrical biphasic articular cartilage layers, *J. Biomech.*, 1995, **28**, 1341-1355.

13 R. Krishnan, E. N. Mariner, G. A. Ateshian, Effect of dynamic loading on the frictional response of bovine articular cartilage, *J. Biomech.*, 2005, **38**, 1665-1673.

14 G. Binnig, C. F. Quate, and C. Gerber, Atomic Force Microscope, *Phys. Rev. Lett.*, 1986, **56**, 930-933.

15 J. N. Israelachvili, Adhesion forces between surfaces in liquids and condensable vapours, *Surf. Sci. Rep.*, 1992, **14**, 109.

16 Y. Dong, Q. Li, A. Martini, Molecular dynamics simulation of atomic friction: A review and guide, *J. Vac. Sci. Technol. A*, 2013, **31**, 030801.

17 B. Q. Luan, S. Hyun, J. F. Molinari, N. Bernstein, and M. O. Robbins, Multiscale modeling of two-dimensional contacts, *Phys. Rev. E*, 2006, **74**, 046710.

18 M. Wolloch, G. Levita, P. Restuccia, and M. C. Righi, Interfacial Charge Density and Its Connection to Adhesion and Frictional Forces, *Phys. Rev. Lett.*, 2018, **121**, 026804.

19 L. Prandtl, Ein Gedankenmodell zur kinetischen Theorie der festen Körper, *Z. Angew. Math. Mech.*, 1928, **8**, 85.

20 G. A. Tomlinson, A molecular theory of friction, *Philos. Mag.*, 1929, **7**, 905.

21 V. L. Popov and J. A. T. Gray, Prandtl-Tomlinson model: History and applications in friction, plasticity, and nanotechnologies, *Z. Angew. Math. Mech.*, 2012 **92**, 683-708.

22 U. D. Schwarz and H. Hölscher, Exploring and Explaining Friction with the Prandtl-Tomlinson Model, *ACS Nano*, 2016, **10**, 38-41.

23 Y. Sang, M. Dubé, and M. Grant, Thermal Effects on Atomic Friction, *Phys. Rev. Lett.*, 2001, **87**, 174301.

24 E. Riedo, E. Gnecco, R. Bennewitz, E. Meyer, and H. Brune, Interaction Potential and Hopping Dynamics Governing Sliding Friction, *Phys. Rev. Lett.*, 2003, **91**, 084502.

25 S. Yu. Krylov, K. B. Jinesh, H. Valk, M. Dienwiebel, and J. W. M. Frenken, Thermally induced suppression of friction at the atomic scale, *Phys. Rev. E*, 2005, **71**, 065101(R).

26 S. Yu Krylov, and J. W. M. Frenken, The crucial role of temperature in atomic scale friction, *J. Phys.: Condens. Matter*, 2008, **20**, 354003.

27 K. B. Jinesh, S. Yu. Krylov, H. Valk, M. Dienwiebel, and J. W. M. Frenken, Thermolubricity in atomic-scale friction, *Phys. Rev. B*, 2008, **78**, 155440.

28 L. Jansen, H. Hölscher, H. Fuchs, and A. Schirmeisen, Temperature Dependence of Atomic-Scale Stick-Slip Friction, *Phys. Rev. Lett.*, 2010, **104**, 256101.

29 D. Perez, Y. Dong, A. Martini, and A. F. Voter, Rate theory description of atomic stick-slip friction, *Phys. Rev. B*, 2010, **81**, 245415.

30 Martin H. Müser, Velocity dependence of kinetic friction in the Prandtl-Tomlinson model, *Phys. Rev. B*, 2011, **84**, 125419.

31 Y. Dong, A. Vadakkepatt, A. Martini, Analytical Models for Atomic Friction, *Tribol. Lett.*, 2011, **44**, 367-386.

32 P. C. Torche, T. Polcar, and O. Hovorka, Thermodynamic aspects of nanoscale friction, *Phys. Rev. B*, 2019, **100**, 125431.

33 A. Socoliuc, R. Bennewitz, E. Gnecco, and E. Meyer, Transition from Stick-Slip to Continuous Sliding in Atomic Friction: Enter-

ing a New Regime of Ultralow Friction, *Phys. Rev. Lett.*, 2004, **92**, 134301.

34 O. M. Braun and Yu. S. Kivshar, Nonlinear dynamics of the Frenkel–Kontorova model, *Physics Reports*, 1998, **306**, 1-108.

35 O. M. Braun and Yu. S. Kivshar, *The Frenkel-Kontorova Model: Concepts, Methods, and Applications*, Springer, Berlin, 2004.

36 T. E. Angelini, A. C. Dunn, J. M. Uruena, D. J. Dickrell, D. L. Burris, and W. G. Sawyer, Cell friction, *Faraday Discuss.*, 2012, **156**, 31-39.

37 B. Ladoux, and R.-M. Mège, Mechanobiology of collective cell behaviours, Nature Reviews, *Moleculer Cell Biology*, 2017, **18**, 743-757.

38 F. Ziebert, and I. S. Aranson, Effects of Adhesion Dynamics and Substrate Compliance on the Shape and Motility of Crawling Cells, *PLoS ONE*, 2013, **8**, e64511.

39 P. S. De, and R. De, Stick-slip dynamics of migrating cells on viscoelastic substrates, *Phys. Rev. E*, 2019, **100**, 012409.

40 K. Hennig, I. Wang, P. Moreau, L. Valon, S. DeBeco, M. Coppey, Y. A. Miroshnikova, C. Albiges-Rizo, C. Favard, R. Voituriez, M. Balland, Stick-slip dynamics of cell adhesion triggers spontaneous symmetry breaking and directional migration of mesenchymal cells on one-dimensional lines, *Science Advances*, 2020, **6**, eaau5670.

41 C. Müller, and T. Pompe, Distinct impacts of substrate elasticity and ligand affinity on traction force evolution, *Soft Matter*, 2016, **12**, 272-280.

42 C.-M. Lo, H.-B. Wang, M. Dembo, and Y.-L. Wang, Cell Movement Is Guided by the Rigidity of the Substrate, *Biophysical Journal*, 2000, **79**, 144-152.

43 M. R. Ng, A. Besser, G. Danuser, and J. S. Brugge, Substrate stiffness regulates cadherin-dependent collective migration through myosin-II contractility, *J. Cell Biol.*, 2012, **199**, 545-563.

44 D. Garcia-Gonzalez, A. Muñoz-Barrutia, Computational insights into the influence of substrate stiffness on collective cell migration, *Extreme Mechanics Letters*, 2020, **40**, 100928.

45 I. Pi-Jaumà, R. Alert, and J. Casademunt, Collective durotaxis of cohesive cell clusters on a stiffness gradient, *Eur. Phys. J. E*, 2022 **45**, 7.

46 L. Trichet, J. Le Digabel, R. J. Hawkins, S. R. K. Vedula, M. Gupta, C. Ribrault, P. Hersen, R. Voituriez, and B. Ladoux, Evidence of a large-scale mechanosensing mechanism for cellular adaptation to substrate stiffness, *PNAS*, 2012 **109**, 6933-6938.

47 P. Sens, Rigidity sensing by stochastic sliding friction, *Europhysics Letters*, 2013 **104**, 38003.

48 K. Vazquez, A. Saraswathibhatla, and J. Notbohm, Effect of substrate stiffness on friction in collective cell migration, *Scientific Reports*, 2022 **12**, 2474.

49 S. Garcia, E. Hannezo, J. Elgeti, J.-F. Joanny, P. Silberzan, and N. S. Gov, Physics of active jamming during collective cellular motion in a monolayer, *PNAS*, 2015, **112**, 15314-15319.

50 H. E. Balcioglu, L. Balasubramaniam, T. V. Stirbat, B. L. Doss, M.-A. Fardin, R.-M. Mège, and B. Ladoux, A subtle relationship between substrate stiffness and collective migration of cell clusters, *Soft Matter*, 2020 **16**, 1825.

51 D. A. Vargas, I. G. Gonçalves, T. Heck, B. Smeets, L. Lafuente-Gracia, H. Ramon, and H. Van Oosterwyck, Modeling of Mechanosensing Mechanisms Reveals Distinct Cell Migration Modes to Emerge From Combinations of Substrate Stiffness and Adhesion Receptor–Ligand Affinity, *Front. Bioeng. Biotechnol.*, 2020, **8**, 459.

52 C. Fei, S. Mao, J. Yan, R. Alert, H. A. Stone, B. L. Bassler, N. S. Wingreen, and A. Kosmrlj, Nonuniform growth and surface friction determine bacterial biofilm morphology on soft substrates, *PNAS*, 2020, **117**, 7622-7632.

53 H. Chelly, A. Jahangiri, M. Mireux, J. Étienne, D. K. Dysthe, C. Verdier, and P. Recho, Cell crawling on a compliant substrate: A biphasic relation with linear friction, *Int. J. Non-Lin. Mech.*, 2022, **139**, 103897.

54 S. Makarchuk, N. Beyer, C. Gaiddon, W. Grange, P. Hébraud, Holographic Traction Force Microscopy, *Scientific Reports*, 2018, **8**, 3038.

55 A. Fuhrmann, and A. J. Engler, The Cytoskeleton Regulates Cell Attachment Strength, *Biophysical Journal*, 2015, **109**, 57-65.

56 L. F. Boesel, C. Greiner, E. Arzt, A. del Campo, Gecko-inspired surfaces: a path to strong and reversible dry adhesives. *Adv. Mater.*, 2010, **22**, 2125-2137.

57 A. del Campo, C. Greiner, I. Alvarez, E. Arzt, Patterned surfaces with pillars with controlled 3d tip geometry mimicking bioattachment devices, *Adv. Mater.*, 2007, **19**, 1973-1977.

58 L. Xue, J. T. Pham, J. Iturri, A. del Campo, Stick-Slip Friction of PDMS Surfaces for Bioinspired Adhesives, *Langmuir*, 2016, **32**, 2428-2435.

59 J. Israelachvili, Y. Min, M. Akbulut, A. Alig, G. Carver, W. Greene, K. Kristiansen, E. Meyer, N. Pesika, K. Rosenberg, H. Zeng, Recent advances in the surface forces apparatus (SFA) technique, *Rep. Prog. Phys.*, 2010, **73**, 036601.

60 D. W. Lee, X. Banquy, and J. N. Israelachvili, Stick-slip friction and wear of articular joints, *PNAS*, 2013, 110, E567-E574.

61 C. J. Rand and A. J. Crosby, Friction of soft elastomeric wrinkled surfaces, *J. Appl. Phys.*, 2009, **106**, 064913.

62 D. Gueorguiev, E. Vezzoli, A. Mouraux, B. Lemaire-Semail, and J.-L. Thonnard, The tactile perception of transient changes in friction, *J. R. Soc. Interface*, 2017, **14**, 20170641.

63 L. Skedung, K. L. Harris, E. S. Collier, M. W. Rutland, The finishing touches: the role of friction and roughness in haptic perception of surface coatings, *Experimental Brain Research*, 2020, **238**, 1511-1524.

64 T.-H. Yang, J. R. Kim, H. Jin, H. Gil, J.-H. Koo, and H. J. Kim, Recent Advances and Opportunities of Active Materials for Haptic Technologies in Virtual and Augmented Reality, *Adv. Funct. Mater.*, 2021 **31**, 2008831.

65 Y. Peng, C. M. Serfass, A. Kawazoe, Y. Shao, K. Gutierrez, C. N. Hill, V. J. Santos, Y. Visell, and L. C. Hsiao, Elastohydrodynamic friction of robotic and human fingers on soft micropatterned substrates, *Nature Materials*, 2021, **20**, 1707-1711.

66 S. Giordano, Spin variable approach for the statistical mechanics of folding and unfolding chains, *Soft Matter*, 2017, **13**,

6877-6893.

67 M. Caruel and L. Truskinovsky, Statistical mechanics of the Huxley-Simmons model, *Phys. Rev. E*, 2016, **93**, 062407.

68 M. Caruel, L. Truskinovsky, Physics of muscle contraction, *Rep. Prog. Phys.*, 2018, **81**, 036602.

69 M. Benedito, S. Giordano, Thermodynamics of small systems with conformational transitions: the case of two-state freely jointed chains with extensible units, *J. Chem. Phys.*, 2018, **149**, 054901.

70 M. Benedito, S. Giordano, Isotensional and isometric force-extension response of chains with bistable units and Ising interactions, *Phys. Rev. E*, 2018, **98**, 052146.

71 G. Florio, G. Puglisi, Unveiling the influence of device stiffness in single macromolecule unfolding, *Sci. Rep.*, 2019, **9** 4997.

72 L. Bellino, G. Florio, and G. Puglisi, The influence of device handles in single-molecule experiments, *Soft Matter*, 2019, **15**, 8680-8690.

73 R. Jorge Do Marco and S. Giordano, Thermodynamics of Extra-Toughness and Hidden-Length in Polymeric Materials with Sacrificial Bonds, *Appl. Mech.*, 2022, **3**, 935-955.

74 G. Florio, G. Puglisi, and S. Giordano, Role of temperature in the decohesion of an elastic chain tethered to a substrate by onsite breakable links, *Phys. Rev. Research*, 2020, **2**, 033227.

75 A. Cannizzo, G. Florio, G. Puglisi, and S. Giordano, Temperature controlled decohesion regimes of an elastic chain adhering to a fixed substrate by softening and breakable bonds, *J. Phys. A: Math. and Theor.*, 2021, **54**, 445001.

76 L. Bellino, G. Florio, S. Giordano, and G. Puglisi, On the competition between interface energy and temperature in phase transition phenomena, *Appl. Eng. Sci.*, 2020, **2**, 100009.

77 A. Cannizzo, L. Bellino, G. Florio, G. Puglisi, and S. Giordano, Thermal control of nucleation and propagation transition stresses in discrete lattices with non-local interactions and non-convex energy, *Eur. Phys. J. Plus*, 2022, **137**, 569.

78 S. Giordano, Statistical mechanics of rate-independent stick-slip on a corrugated surface composed of parabolic wells, *Continuum Mechanics and Thermodynamics*, 2022, **34**, 1343-1372.

79 A. Prados, A. Carpio, and L. L. Bonilla, Sawtooth patterns in force-extension curves of biomolecules: An equilibrium-statistical-mechanics theory, *Phys. Rev. E*, 2013, **88**, 012704.

80 L. L. Bonilla, A. Carpio, and A. Prados, Theory of force-extension curves for modular proteins and DNA hairpins, *Phys. Rev. E*, 2015, **91**, 052712.

81 D. De Tommasi, N. Millardi, G. Puglisi, and G. Saccomandi, An energetic model for macromolecules unfolding in stretching experiments, *J. R. Soc. Interface*, 2013, **10**, 20130651.

82 I. Benichou and S. Givli, Structures undergoing discrete phase transformation, *J. Mech. Phys. Sol.*, 2013, **61**, 94.

83 F. Manca, S. Giordano, P. L. Palla, R. Zucca, F. Cleri, and L. Colombo, Elasticity of flexible and semiflexible polymers with extensible bonds in the Gibbs and Helmholtz ensembles, *J. Chem. Phys.*, 2012, **136**, 154906.

84 J. H. Weiner, *Statistical Mechanics of Elasticity*, Dover Publications, New York, 1983.

85 V. Aleshin, K. Van Den Abeele, Friction in unconforming grain contacts as a mechanism for tensorial stress–strain hysteresis, *J. Mech. Phys. Sol.*, 2007, **55**, 765-787.

86 J. Wojewoda, A. Stefański, M. Wiercigroch and T. Kapitaniak, Hysteretic effects of dry friction: modelling and experimental studies, *Phil. Trans. R. Soc. A*, 2008, **366**, 747-765.

87 J. T. Oden, and E. B. Pires, Nonlocal and Nonlinear Friction Laws and Variational Principles for Contact Problems in Elasticity, *J. Appl. Mech.*, 1983, **50**, 67-76.

88 D. Jelagin, P.-L. Larsson, Nonlocal Frictional Effects at Indentation of Elastic Materials, *Tribol. Lett.*, 2013, **51**, 397-407.

89 R. A. Usmani, Inversion of a tridiagonal Jacobi matrix, *Linear Algebra Its Appl.*, 1994, **212/213**, 413.

90 R. A. Usmani, Inversion of Jacobi's tridiagonal matrix, *Computers Math Applic.*, 1994, **27**, 59.

91 E. T. Whittaker, G. N. Watson, *A Course of Modern Analysis*, Cambridge University Press, Cambridge UK, 2021.

92 I. S. Gradshteyn and I. M. Ryzhik, *Table of Integrals, Series and Products*, Academic Press, San Diego, 1965.

93 M. Abramowitz, I.A. Stegun, *Handbook of Mathematical Functions*, Dover Publication, New York, 1970.

94 F.W.J. Olver, D.W. Lozier, R.F. Boisvert, C.W. Clark, *NIST Handbook of Mathematical Functions*, National Institute of Standards and Technology and Cambridge University Press, New York, 2010.

95 R. Bellman, *A brief introduction to theta functions*, Holt, Rinehart and Co., New York, 1961.

96 G. E. Andrews, Ramanujan's "lost" notebook. I. Partial θ-functions, *Adv. Math.*, 1981, **41**, 137-172.

97 G. E. Andrews, Ramanujan's "lost" notebook. II. θ-function expansions, *Adv. Math.*, 1981, **41**, 173-185.

98 S. O. Warnaar, Partial Theta Functions. I. Beyond the Lost Notebook, *Proceedings of the London Mathematical Society*, 2003, **87**, 363-395.

99 M. Z. Baykara, M. R. Vazirisereshk, and A. Martini, Emerging superlubricity: A review of the state of the art and perspectives on future research, *Appl. Phys. Rev.*, 2018, **5**, 041102.

100 A. Kumar, Advancements in emerging superlubricity: A review of the atomistic models, simulation techniques and their applications to explore the state of ultra-low friction, *Materials Today: Proceedings*, 2021, **42**, 884-892.

101 X. Zhao, S. R. Phillpot, W. G. Sawyer, S. B. Sinnott, and S. S. Perry, Transition from Thermal to Athermal Friction under Cryogenic Conditions, *Phys. Rev. Lett.*, 2009, **102**, 186102.

102 I. Barel, M. Urbakh, L. Jansen and A. Schirmeisen, Multi-bond Dynamics of Nanoscale Friction: The Role of Temperature, *Phys. Rev. Lett.*, 2010, **104**, 066104.

103 H. Risken, *The Fokker-Planck equation*, Springer Verlag, Berlin, 1989.

104 W. T. Coffey, Yu. P. Kalmykov, and J. P. Waldron, *The Langevin equation*, World Scientific, Singapore, 2004.

105 I. Benichou, S. Givli, Rate Dependent Response of Nanoscale Structures Having a Multiwell Energy Landscape, *Phys. Rev. Lett.*, 2015, **114**, 095504.

106 I. Benichou, Y. Zhang, O. K. Dudko, S. Givli, The rate dependent response of a bistable chain at finite temperature, *J. Mech. Phys. Sol.*, 2016, **95**, 44.

107 F. Manca, P.-M. Déjardin, S. Giordano, Statistical mechanics of holonomic systems as a Brownian motion on smooth manifolds, *Annalen der Physik (Berlin)*, 2016, **528**, 381-393.

108 S. Giordano, Stochastic thermodynamics of holonomic systems, *Eur. Phys. J. B*, 2019, **92**, 174.